Evolutionary algorithm based controller for double link flexible robotic manipulator

J. Annisa[1], I.Z. Mat Darus[1,*], M.O. Tokhi[2]

[1)] Faculty of Mechanical Engineering, Universiti Teknologi Malaysia, Skudai, 81310, Johor Bahru, Malaysia
[2)] London South Bank University, 103 Borough Road, London, United Kingdom

[*]Corresponding e-mail: annisajamali@gmail.com

Keywords: Flexible manipulator; artificial bee colony; particle swarm optimization

ABSTRACT –The paper investigates the development of intelligent hybrid collocated and non-collocated PID controller for hub motion and end point vibration suppression of double-link flexible robotic manipulator. The system was modeled using multi-layer perceptron neural network structure based on Nonlinear Autoregressive Exogenous (NARX) model. The hybrid controllers are incorporated with optimization algorithm that is ABC and PSO to find out the parameters of the PID controllers. Numerical simulation was carried out in MATLAB/Simulink to evaluate the system in term of tracking capability and vibration suppression for both links. The results show that PSO revealed the superiority over ABC in controlling the system.

1. INTRODUCTION

Despite various advantages shown by flexible manipulator such as offers cost reduction, lower power consumption, improved dexterity, better maneuverability, safer operation and light weight, the undesirable vibration is the common shortcoming occurred in the structure. In order to satisfy the conflicting requirements, number of research on improving the control methods have been carried out.

Evolutionary Algorithms have been used in various areas including in developing tuning method of PID controller for flexible manipulator. For instance, hybrid PD-PD/Iterative learning Algorithm (ILA) tuned by Genetic Algorithm for single-link flexible manipulator (SLFM) is presented in [1], a multi-objective optimization using Differential Evolution (MODE) for PID controller of SLFM studied in [2], an improved Bacterial Foraging Algorithms (BFA) to tune the PID controller of SLFM is proposed in [3], Bee Algorithm is used to optimize the hierarchical PID parameter of SLFM in [4] and particle swarm optimization (PSO) algorithm to tune parameter of one PID controller of SLFM in [5].

In this paper, a hybrid PID-PID controller is developed for double link flexible robotic manipulator (DLFR) based on the NARX model plant as elaborated in [6]. The global search of ABC and PSO are utilized to optimize all the PID controllers' gains.

2. CONTROL SCHEME

The control scheme is shown in Fig.1. The PID_{i1} controller is developed for hub angle motion while PID_{i2} controller is applied for flexible body motion. The two loops of each link ($i=1,2$) are combined together to give control inputs that work simultaneously for the DLFR.

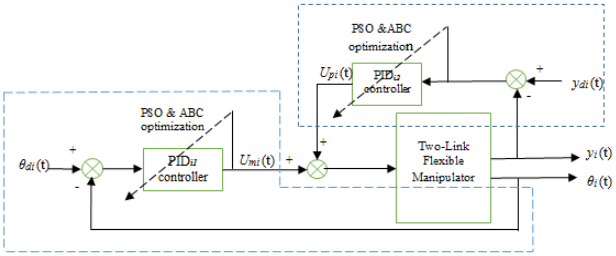

Figure 1 Hybrid controller structure of double link flexible robotic manipulator.

2.1 Controller design

The proposed control structure using novel evolutionary algorithms of PSO and ABC to tune the PID controllers' parameters. The objective functions of optimization are formulated based on the MSE of the hub angle error and end point vibration suppression. The details of algorithm as follow.

2.1.1 Particle Swarm Optimization (PSO)

PSO is initialized with a group of random particles and then searches for optimum by updating generations. The particle updates its velocity and positions with following Eq. (1) and (2).

$$V_{id}^{k+1} = W * V_{id}^{k} + C1 * R1 * \left(Y_{id}^{k} - X_{id}^{k}\right) + C2 * R2 * \left(Y_{id}^{k} - X_{id}^{k}\right) \quad (1)$$

$$X_{id}^{k+1} = Y_{id}^{k} - X_{id}^{k} \quad (2)$$

where V= particle velocity, X= particle position, W= Inertia weight, R_1, R_2 = random number and C_1, C_2 = learning factors. In this research, $C_1 = C_2$ is chosen as 2 and R_1, R_2 is between 0 and 1. The starting and end point of inertia weight, W set as 0.9 and 0.25.

2.1.2 Artificial Bees Colony Algorithm (ABC)

ABC is inspired by intelligent behavior of honey bees to look for the best food location. The fitness is calculated by the following formula (3), after that a greedy selection is applied between x_m and v_m.

$$fit_m(x_m) = \frac{1}{1 + f_m(x_m)}, f_m(x_m) > 0$$

$$fit_m(x_m) = 1 + |f_m(x_m)|, f_m(x_m) < 0 \quad (3)$$

where $f_m(x_m)$ is the objective function value of x_m. The quantity of a food source is evaluated by its profitability.

P_m is determined by the formula;

$$P_m = \frac{fit_m(x_m)}{\sum_{m=1}^{SN} fit_m(x_m)} \quad (4)$$

where, $fit_m(x_m)$ is the fitness of x_m. If the fitness value of is better than that of its parent, then update with otherwise keep unchanged.

3. RESULTS AND DISCUSSION

3.1 Hub angle control

The hub angles were controlled by the collocated PID controller individually. The DLFR system is required to follow a step input of 2.1 rad and 1.1 rad to test the hub tracking input of link 1 and 2 respectively. The controller parameters obtained and their performances are tabulated in Table 1.

Table 1 Parameters and performance of hub input tracking for DLFR system.

		Parameters			Rise Time (s)	Sett. Time (s)	Over shoot (%)
		K_P	K_I	K_D			
ABC	L 1	6.54	20.5	49.43	0.076	1.08	1.94
	L 2	5.48	28.3	13.72	0.099	5.64	3.19
PSO	L1	3.65	57.9	3.46	0.058	1.16	0.89
	L 2	2.19	88.2	0.79	0.04	0.59	1.64
ZN	L1	2.09	0.54	2.01	2.97	7.15	4.69
	L2	4.15	1.3	3.32	1.46	5.45	5.45

The hub angle response for both link is shown in Fig. 2. PSO and ABC controller achieved a very significance improvement in term of percentage overshoot and settling time as compared to Ziegler-Nichols (ZN). However, in overall PSO lead the ABC in giving better results.

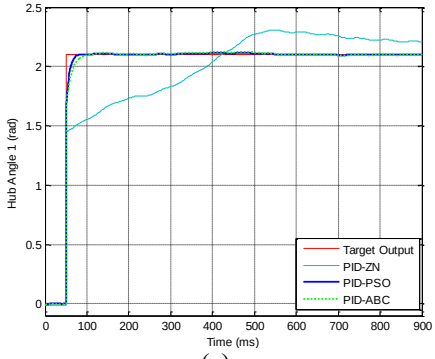

(a)

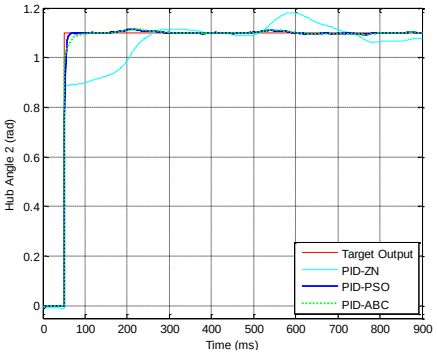

(b)

Figure 2 (a) Input tracking for Hub 1 (b) Input tracking for Hub 2.

3.2 Flexible motion control

The collocated PID controllers were implemented to DLFR system to actively suppress the vibration at the end point of link 1 and 2 individually. The results are tabulated in Table 2 and the simulation results of vibration suppression are presented in Fig. 3. The vibration can be further suppressed by employing the ABC and PSO controller as compared to ZN. Overall, PSO shows the superiority over ABC.

Table 2 Parameters and performance of vibration suppression for DLFR system.

		Parameters			MSE
		K_P	K_I	K_D	
ABC	L1	30.03	56.07	88.95	7.919e-07
	L2	50.1	46.96	23.62	8.432e-08
PSO	L 1	2.07	498.1	2.04	3.948e-08
	L 2	8.06	817.9	1.03	4.315e-08
ZN	L1	7.2	21.176	0.612	2.822e-06
	L2	16	55.082	1.281	7.564e-07

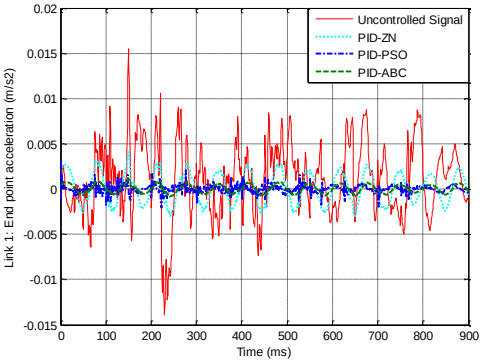

(a)

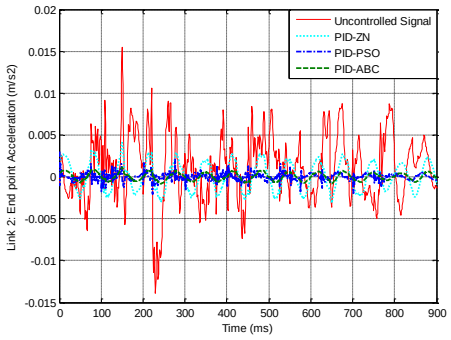

(b)

Figure 3 (a) End point vibration suppression of Hub 1(b) End point vibration suppression of Hub 2.

4. CONCLUSION

In this work, the intelligent Hybrid PID-PID controllers have been developed for DLFR. The controllers have been compared with hybrid PID-ZN controller. The proposed control schemes have been tested through simulation in Matlab/Simulink environment. The proposed controllers are able to follow the reference trajectory and the vibration of the system is eliminated simultaneously through end point acceleration feedback. However, it is revealed that PSO controllers offer the best outcomes compared to ABC.

ACKNOWLEDGEMENT

The authors would like to express their gratitude to Minister of Education Malaysia (MOE), Universiti Teknologi Malaysia (UTM) and Universiti Malaysia Sarawak (UNIMAS) for funding and providing facilities to conduct this research.

REFERENCES

[1] M.S. Alam, M.Z. Md Zain, M.O. Tokhi and F. Aldebrez, "Design of hybrid learning control for flexible manipulators: A multi-objective optimisation approach," in *Proceedings of CLAWAR,* 2006, pp. 599–606.

[2] I.B. Tijani, R. Akmeliawati, A.G.A. Muthalif and A. Legowo, "Optimization of PID controller for flexible link system using a pareto-based multi-objective differential evolution," in *Proceeding of 4th International Conference on Mechatronics*, 2011.

[3] H. Supriyono, M.O. Tokhi and B.A. Md Zain, "Control of a single-link flexible manipulator using improved bacterial foraging algorithm," in *Proceeding of Conference on Open Systems,* 2010, pp. 68–73.

[4] A.A. Fahmy, M. Kalyoncu and M. Castellani, "Automatic design of control systems for robot manipulators using the bees algorithm," *Journal of Systems and Control Engineering,* vol.1, pp. 1–12, 2011.

[5] H. Yatim and I.Z. Mat Darus, "Self-tuning active vibration controller using particle swarm optimization for flexible manipulator system," *WSEAS Transactions on Systems and Control,* vol. 9, pp.55–66, 2011.

[6] A. Jamali, I.Z. Mat Darus, A. Abdulhussain and M.O. Tokhi, "Non-parametric modeling of double link flexible robot manipulator," *in Proceeding of CLAWAR,* 2016, pp.559-566.

Wiper noise and vibration on designated test facility

I. Salleh[1], M.Z. Md Zain[1,*], A.R. Abu Bakar[1], Z. Mohamed[2]

[1)] Faculty of Mechanical Engineering, Universiti Teknologi Malaysia, Skudai, 81310, Johor Bahru, Malaysia
[2)] Faculty of Electrical Engineering, Universiti Teknologi Malaysia, Skudai, 81310, Johor Bahru, Malaysia

[*]Corresponding e-mail: zarhamdy@mail.fkm.utm.my

Keywords: Noise and vibration; wiper system

ABSTRACT - Wiper noise and vibration is a problem in a vehicle that can be annoying and affects the driver concentration during driving**.** This paper will show the measurement of wiper noise and vibration on a specially designated wiper test facility using a pair of MMA7660 accelerometer and the data was processed by ADVANTECH USB-4716: Portable Data Acquisition Module. It will be tested on wet and dry condition at three wiper operation levels; moderate, fast and intermittent. The vibration will be shown in term of frequency behaviour to determine the type of noise; squeal, chattering or reversal, that produced by the wiper system.

1. INTRODUCTION

The wiper system main function is sweeping rain, fog, dirt and other contaminants that stick on the windscreen to give a clear sight for comfortable driving condition and secure driver and passenger safety. One of the concerns on the wiper is wiper noise and vibration as it can be annoying and affect the driver concentration during driving [1]. The friction between the rubber blade and windscreen is one of the main sources of noise and vibration. These noises divided into three levels; squeal, chattering and reversal noise. Squeal or squeaky noise is a high frequency noise generated at about 1000Hz. Meanwhile, reversal noise, a mid-frequency noise is produces at about 500Hz [2]. The low-frequency noise, chattering noise generated at 100Hz [3]. The development of the wiper system test facility was to measure and categorized the noise. Using the data from this test, researcher can easily access the wiper system for further change to achieve the main objective which is to reduce noise and vibration and implement it into the wiper system.

2. METHODOLOGY

Three procedures were conducted. Firstly, the design and fabrication process of the wiper test facility. Then, the test facility needs to be setup based on the ISO 9259:1991 - Passenger Cars - Windscreen Wiper System – Wiper Arm – to - blade connection standard before proceed with the measurement of noise and vibration.

2.1 Design and fabrication of test facility

The designated test facility needs to operate the same as the wiper system install on the vehicle. The test facility was an assembly of wiper system of passenger car and installed it on the fabricated steel frame. As for the wiper system, the parts that was taken from the vehicle and installed to the frame were windscreen, wiper motor and linkage system and wiper controller. Figure 1 shows the finishes test facility of the wiper system that used for the noise and vibration measurement.

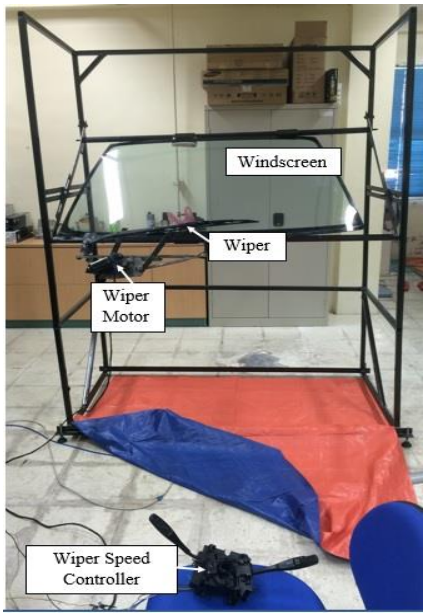

Figure 1 Wiper system test facility.

2.2 Wiper system requirement based on ISO 9259:1991 - Passenger cars - Windscreen wiper system – Wiper arm to blade connection

Before proceed with the measurement, the test facility setup needs to follow ISO 9259:1991 standard. The requirement divides into two categories; wiper system condition and wiper blade condition. For the wiper system condition, it's including wiping area, frequency, durability, accessibility and intermittent operation and for the wiper blade is durability and wiper quality.

As for blade durability, it must remain functional after operating 1.5 million cycles. The wiper blade element shall wipe effectively 500 000 cycles of the 3,000 000 system test. The wiper blade shall clear the entire wipe pattern within one wiping cycle with only minor streaking or unwiped lines remaining for wipe quality. Once the following standard followed and fulfilled, the measurement of wiper noise and vibration on the wiper system can be done.

2.3 Measurement of noise and vibration

In order to measure and analyze the noise and vibration on the wiper system, a pair of MMA7660 accelerometer single axis was used and the data was process by ADVANTECH USB-4716: Portable Data Acquisition Module as shown in Figure 2. The accelerometer was attached at the primary yoke of the uni-blade type of wiper to measure the vibration. The measurement was test at three operation levels of wiper system which is intermittent, moderate and fast.

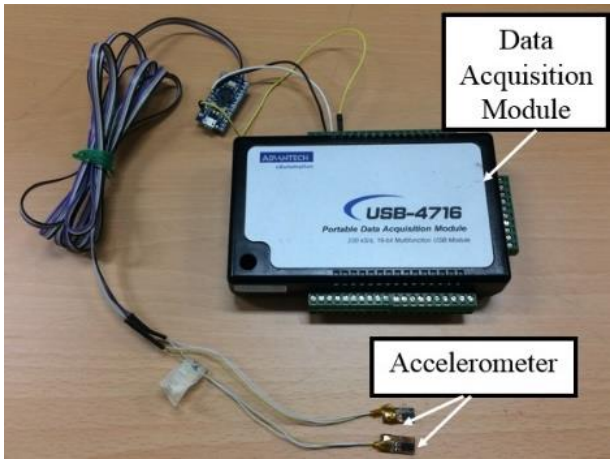

Figure 2 MMA7660 accelerometer and ADVANTECH USB-4716.

3. RESULTS AND DISCUSSION

Figure 3 shows the frequency range of the wiper vibration for dry condition at three wiper operation levels with sampling rate of 512 per seconds. The dominant frequency for all wiper operation levels is below 10 Hz. The highest frequency recorded is 9.69Hz and the lowest is 0.17Hz.

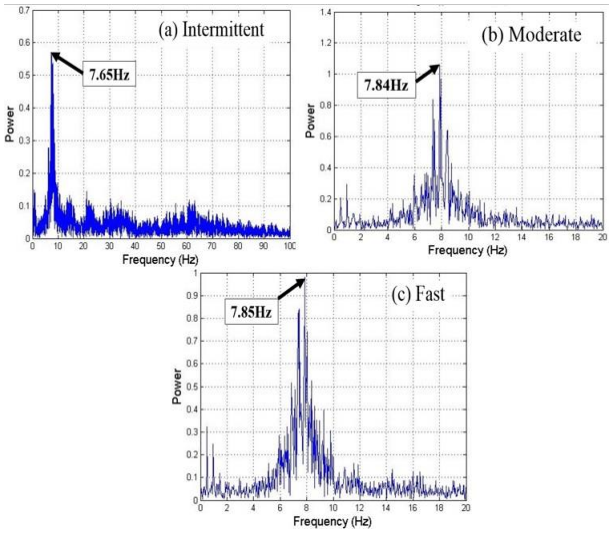

Figure 3 Wiper vibration frequency behaviour during dry test.

Figure 4 shows the frequency range of the wiper vibration for wet condition at three wiper operation levels using the same sampling rate of 512 per seconds. From the figure, the dominant frequency is in the range below 10Hz with the highest frequency is at 7.85Hz and the lowest is 7.65Hz. The different is the level of power produce by the vibration.

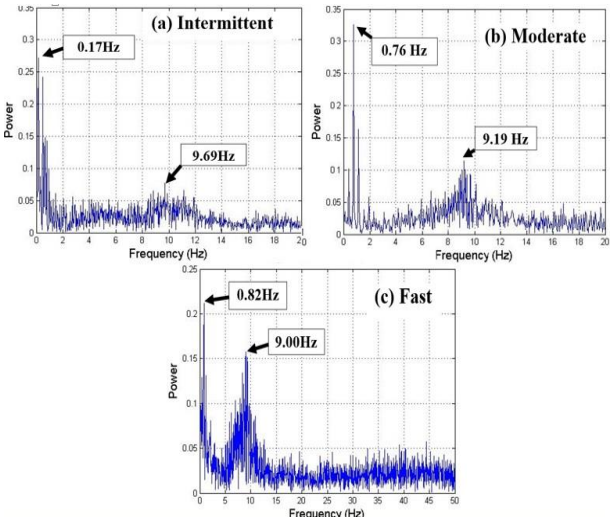

Figure 4 Wiper vibration frequency behaviour during wet test.

The frequency behaviour indicated that the tested wiper system only produced chatter noise that ranging below 100Hz as proved from previous study and has been done on wiper system on real vehicle [4].

4. CONCLUSIONS

The wiper produces a low frequency vibration and noise called chatter noise at different condition and operating levels. Regardless the condition and operation levels, chattering noise is generated before and after wiper turnover. For further research, a proper controller will be proposed to reduce the vibration effect on the wiper system. The purposed of this test facility is for easily access compared to wiper system install in vehicle for further analysis. So, the test facility can be replaced wiper system in the vehicle.

REFERENCES

[1] S. Goto, H. Takahashi and T. Oya, “Investigation of wiper blade squeal noise reduction measures,” *SAE Technical Paper*, pp. 1-87, 2001.

[2] S. Goto, H. Takahashi and T. Oya, “Clarification of the mechanism of wiper blade rubber squeal noise generation,” *JSAE Rev.*, vol. 22, no. 1, pp. 57–62, 2001.

[3] R. Suzuki and K. Yasuda, “Analysis of chatter vibration in an automotive wiper assembly.,” *JSME Int. J. Ser. C*, vol. 41, no. 3, pp. 616–620, 1998.

[4] A. Bakar, E. Jamaluddin and L. Yin, “An experimental investigation into noise and vibration of an automotive wiper,” in *Regional Conference on Noise, Vibration and Comfort (NVC)*, 2007, pp. 261–269.

, Active robust vibration control of a flexible beam

Mohd Fairus Jamid[1,*], Intan Zaurah Mat Darus[1], Mohd Sazli Saad[2]

[1)] Faculty of Mechanical Engineering, Universiti Teknologi Malaysia, 81300 Skudai, Johor Darul Takzim, Malaysia
[2)] School of Mechanical Engineering, Universiti Malaysia Perlis, Arau, Perlis, Malaysia

[*]Corresponding e-mail: mfairusj@gmail.com

Keywords: Robust; vibration; beam

ABSTRACT – This paper presents the experimental studies of an active robust controller to suppress the unwanted vibration of a flexible beam. The vibration is controlled using a piezoelectric actuator bonded on a flexible beam. A constant velocity excitation is given to the system by a steel ball with a certain weight to produce free vibration. The experimental results showed that the proposed control method is efficient for vibration suppression.

1. INTRODUCTION

Flexible structures are widely used in various applications such as aerospace, manufacturing process, automation, etc. Due to the flexibility and lightweight of these structures the problem of structural vibration arises, thus the need for vibration control of these structures become important [1-5]. In recent years, the studies in active vibration control become more extensive in suppressing the unwanted structural vibration and improve the performance of flexible structures. Tokhi and Hossain [2] presented the study on active vibration control (AVC) algorithm based on active noise control method. The AVC was realized in a similar manner as active noise control. Later, Hu and Ng [1] presented an active robust method for controlling unwanted vibration suppressing of a circular plate.

This paper, therefore presents a study on the robustness of a control system tested experimentally using real time AVC control algorithm. The beam was subjected to external disturbances with a certain weight in order to give more comprehensive information.

2. THE ACTIVE VIBRATION CONTROL

Figure 1 shows a schematic diagram of the arrangement of the AVC structure. Primary force was introduced to the beam to create unwanted vibration. This unwanted vibration is detected by a detector. Then, the detected signal is fed to a controller and processed to produce suitable control signal. This signal is later fed to a secondary source as a cancelling source at a desired location. The secondary signal thus generated is superimposed on the primary signal cancel the vibration reduction at the observation point [1-2].

The objective of the scheme in Figure 1 is to achieve the optimum vibration attenuation at the observation point. To develop an AVC system with the controller characteristics which are updated in accordance with changes in the system, a self-tuning strategy, allowing the online implementation of the controller can be utilized. This requires the primary and secondary signals at the observation point to be equal in amplitude but having a phase difference of 180° relative to one another. Synthesizing the controller on the basis of this objective yields [2-4]:

$$C = \left[1 - \frac{Q_1}{Q_0}\right]^{-1} \quad (1)$$

where, Q_0 and Q_1 represent the equivalent transfer functions of the system (with input at the detector and output at the observation) when the secondary source is off and on respectively. Equation (1) is the required controller design rule which can easily be implemented on-line using digital processor. The process of identification of Q_0 and Q_1 was using RLS algorithm. The process of control, on the other hand, involves designing the controller according to Equation (1) and implementing this in real-time [5].

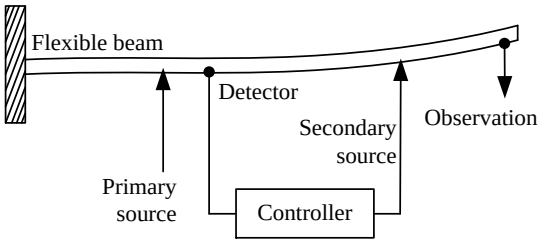

Figure 1 Schematic diagram of the AVC system.

2.1 Experimental setup

To implement the AVC to the beam system an aluminum type of metal with size of (450 x 50 x 1.4) mm was considered. Two piezoelectric patches were surface bonded to the beam that act as primary and secondary source actuators. Two laser displacement sensors were used to measure the beam deflection with range 50 ± 10mm as a detector and observer. This experiment was conducted in non-collocated control where the locations of the sensor and the control actuator are not in the same position as shown in Figure 2.

The RLS based AVC control algorithm was developed with LabVIEW programming software which is suitable for computer control application where interfacing between input-output and the computer system can be done easily using National Instruments data acquisition card. The sampling rate for the acquisition system was set to 1 kHz which is enough to capture the data with 1000 samples per second [6].

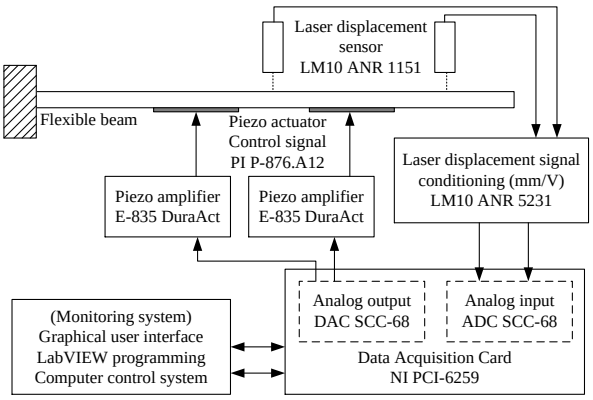

Figure 2 Experimental setup.

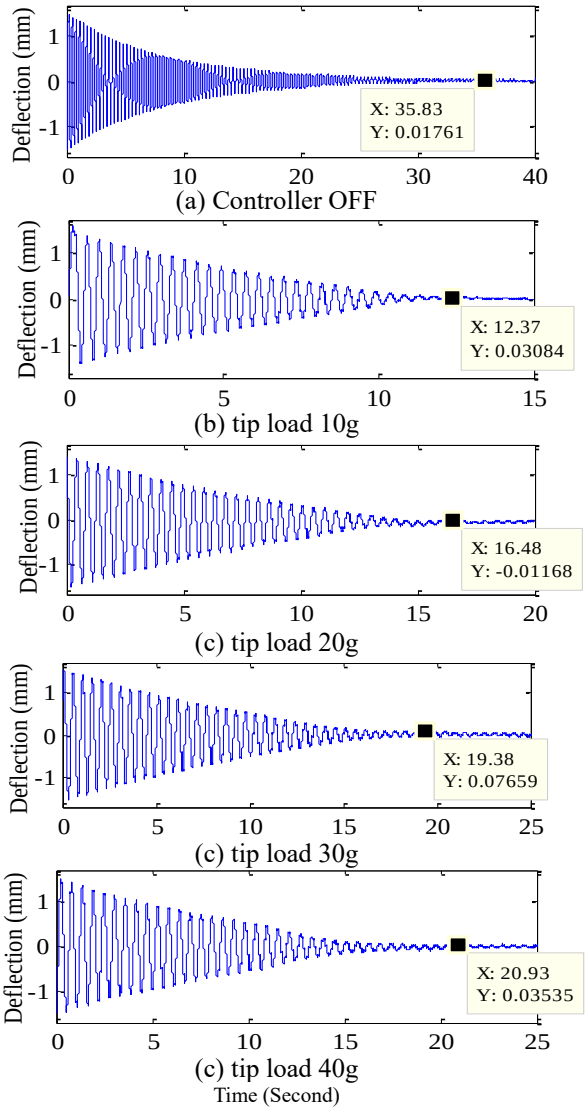

Figure 3 Experiment time performance.

3. RESULTS AND DISCUSSION

An experimental rig was designed and developed to investigate the robustness of AVC via PC-based control with various tip loads attached on the flexible beam. A steel ball with a certain weight was allowed to swing freely from a certain height, which then impacted on the flexible beam. The transient performance of the AVC algorithm was observed.

Figure 3 shows the comparison of time response of the AVC based controller. The system corresponding to 0-gram tip load was taken as the initial condition, which means no control was applied to the system. For a 0 gram without controller on test, the closed loop settling times is about 35.83s. The performance of the controller is investigated by varying the tip load from 10 grams to 40 grams with the increment of 10 grams. It can be seen that the closed loop settling times for each tip load are from 12.37 s, 16.48 s, 19.38 s and 20.93 s respectively. It can be concluded that the controller has the ability to maintain its performance to suppress the unwanted vibration when there is a physical change on the flexible beam system.

4. CONCLUSIONS

The investigation of active robust controller to suppress unwanted vibration of a flexible beam has been presented. Robustness of the control system has been tested experimentally in real time AVC controller where the beam is subjected to external disturbances with a certain weight. It is shown that the control system able to attenuate the unwanted vibration with different external disturbances.

REFERENCES

[1] Y.R. Hu and A. Ng, "Active robust vibration control of flexible structures," *Journal of Sound and Vibration*, vol. 288, no. 1-2, pp. 43–56, 2005.

[2] M.O. Tokhi and M.A. Hossain, "Self-tuning active vibration control in flexible beam structures," *Proceedings of the Institution of Mechanical Engineers Part I Journal of Systems and Control Engineering*, vol. 208, no. 49, 263–278, 1994.

[3] M.A. Hossain, M.O. Tokhi, A.J. Chipperfield, M.J. Baxter, C.M. Fonseca and N.V. Dakev, "Adaptive active vibration control using genetic algorithms," in *First International Conference on Genetic Algorithms in Engineering Systems: Innovations and Applications,* 1995, pp. 175–180.

[4] I.Z. Mat Darus, and M.O. Tokhi, "Soft computing-based active vibration control of a flexible structure. *Engineering Applications of Artificial Intelligence*, vol. 18, no. 1, 93–114, 2005.

[5] I.Z. Mat Darus and M.O. Tokhi, "Adaptive neuro-active vibration suppression of a flexible plate structure," in *Proceedings of the 2003 10th IEEE International Conference on Electronics, Circuits and Systems*, 2003, pp. 360–363.

[6] M.S. Saad, H. Jamaluddin and I.Z. Mat Darus, "Online monitoring and self-tuning control using pole placement method for active vibration control of a flexible beam. *Journal of Vibration and Control*, vol. 21, no. 3, pp. 449–460, 2013.

PID-VSC controller tuning optimization with PFPSO for 3D gantry crane system

S.Y.S. Hussien[1,2], R. Ghazali[1,2,*], H.I. Jaafar[1,2], C.C. Soon[1,2]

[1)] Faculty of Electrical Engineering, Universiti Teknikal Malaysia Melaka, Hang Tuah Jaya, 76100 Durian Tunggal, Melaka, Malaysia
[2)] Centre for Robotics and Industrial and Automation, Universiti Teknikal Malaysia Melaka, Hang Tuah Jaya, 76100 Durian Tunggal, Melaka, Malaysia

[*]Corresponding e-mail: rozaimi.ghazali@utem.edu.my

Keywords: 3D gantry crane system; variable structure control; priority-based fitness particle swarm optimization

ABSTRACT – The control of three-dimensional (3D) crane system represents one of the most widely challenging control problem. A 3D Gantry Crane System (GCS) is used for lifting and moving loads horizontally, lowering and releasing the gripper to the original position. This paper presents a control strategy of Proportional-Integral-Derivative and Variable Structure Control (PID-VSC) controller tuned by Priority-based Fitness Particle Swarm Optimization (PFPSO). PID controller is used to control the trolley movement reach at the precise desired position while VSC controller is used to control the undesired oscillation from the payload while moving the load. The performance of trolley position and payload oscillation which controlled by PID-VSC controller tuned by PFPSO show a better performance compared to PID-PD controller.

1. INTRODUCTION

Gantry Crane System (GCS) as illustrated in Figure 1 is important in the transportation industry for loading and unloading load. The control objective of this system is to move the trolley to a desired position as fast and accurate as possible without causing any immoderate sway at the final target position. In transportation industry, speed is required as the priority issue as it translates into productivity and efficiency of the system. However, controlling the crane manually by human will tend to excite sway angles of the hoisting line and degrade the overall performance of the system. At very low speed, the payload angle is not significant and can be ignored, but not for high speed condition. The payload oscillation become larger and hard to settle down during movement and unloading.

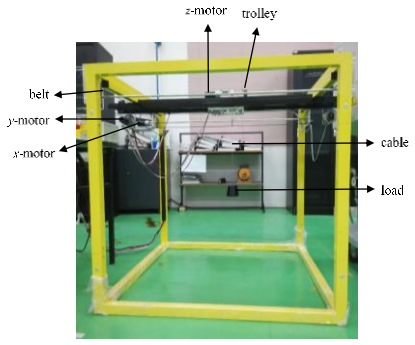

Figure 1 3D INTECO GCS.

This paper presents the implementation of PID controller used to control the trolley movement in order to achieve the desired position whereas VSC used to minimize the oscillation during the movement. Performances of the developed control schemes are accessed in terms of the trolley position and payload oscillation reduction. The simulation results in 3D INTECO GCS which controlled by PID-VSC controller optimized by PFPSO are compared to PID-VSC controller optimized by PSO and PID-PD controller optimized by Zeigler-Nichols (ZN), Particle Swarm Optimization (PSO) and PFPSO.

2. 3D INTECO GANTRY CRANE SYSTEM

Figure 2 shows the schematic representation of 3D INTECO GCS. The dynamic equations of motion in y-direction in for the GCS is obtained as denoted in Equation (1) and Equation (2) where, y_t is the position of trolley and y_p is the position of payload oscillation [1]. The parameters implemented to the GCS are tabulated in Table 1.

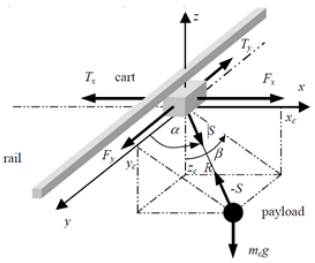

Figure 2 Structure of 3D INTECO GCS.

$$\ddot{y}_t = \left(\frac{F_x}{m_w} - \frac{T_x}{m_w}\right) + \left(\frac{m_c}{m_w}\right)\left(\frac{F_z}{m_c} - \frac{T_z}{m_c}\right)\cos\alpha \quad (1)$$

$$\ddot{y}_p = \ddot{y}_t + \left(\ddot{R} - R\dot{\alpha}^2\right)\cos\alpha - \left(2\dot{R}\dot{\alpha} + R\ddot{\alpha}\right)\sin\alpha \quad (2)$$

3. CONTROL SCHEME

Figure 3 illustrated the block diagram of control scheme in the GCS. In GCS, PID controller is implemented to control the trolley position. Besides, PD and VSC controllers are implemented to control the payload oscillation while moving the payload to the desired position. The parameters in these controllers are optimized by the meta-heuristics method which is

PFPSO with 20 agents and 100 iterations. The priority of performance is set as overshoot (OS) as highest priority, followed by settling time (T_s) and steady-state error (e_{ss}) [2].

Table 1 Parameters of 3D INTECO GCS [1].

Parameters	Unit	Values
Payload mass	m_c	0.46 kg
Trolley mass	m_w	1.16 kg
Moving rail mass	m_s	2.20 kg
Gravity	g	9.81 ms^{-1}
Friction force at x-axis	T_x	100.00 Nsm^{-1}
Friction force at y-axis	T_y	82.00 Nsm^{-1}
Friction force at z-axis	T_z	75.00 Nsm^{-1}
Length of cable	R	0.30 m

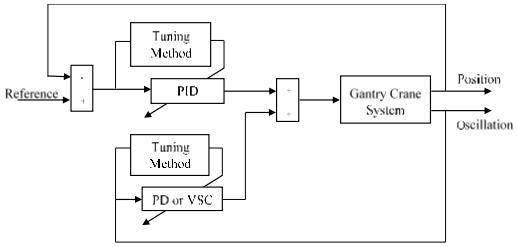

Figure 3 Block diagram of control scheme.

Table 2 Parameters of PID-PD and PID-VSC controllers.

	Tuning Methods				Tuning Methods	
	ZN	PSO	PFPSO		PSO	PFPSO
K_P	3.00	20.97	2.52	K_P	20.94	3.86
K_I	3.00	10.85	0.11	K_I	10.84	0.003
K_D	1.88	4.47	3.04	K_D	0.01	1.93
K_{PS}	4.00	5.01	2.96	k_1	0.02	0.70
K_{DS}	1.10	0.07	0.06	k_2	7.03	9.63

4. RESULTS AND DISCUSSION

The response in trolley position in Figure 4 is clearly seen that the controller optimized by PFPSO shown a good performance in terms of OS with no overshoot. In terms of T_s, PID-VSC controller tuned by PFPSO took an improvement of five seconds faster than PID-PD controller optimized by PFPSO for the system to reach a steady state. Besides, PID-VSC controller optimized by PFPSO shows the smallest error of 0.006×10^{-3} meter. The performances of trolley position is tabulated in Table 3.

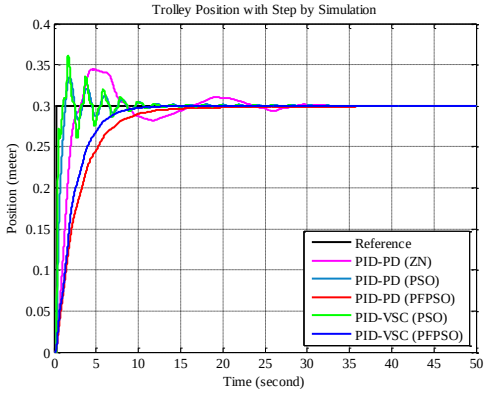

Figure 4 Response of trolley position.

Table 3 Performance in trolley position.

Tuning Methods	Performances		
	OS (%)	T_s (second)	e_{ss} (meter) ($x10^{-3}$)
PID-PD (ZN)	14.733	28.170	0.455
PID-PD (PSO)	11.400	11.530	0.068
PID-PD (PFPSO)	0.000	15.830	0.015
PID-VSC (PSO)	20.267	12.390	0.035
PID-VSC (PFPSO)	0.000	10.830	0.006

Figure 5 shows the payload oscillation in GCS controlled by PID-VSC controller tuned by PFPSO produced 0.039 radian and stopped oscillating at 16.250 seconds compared to another optimization. In this research, PID-VSC controller tuned by PFPSO show the controller able to control and minimize the payload oscillation in GCS faster compared to others. The performance of payload oscillation is tabulated in Table 4.

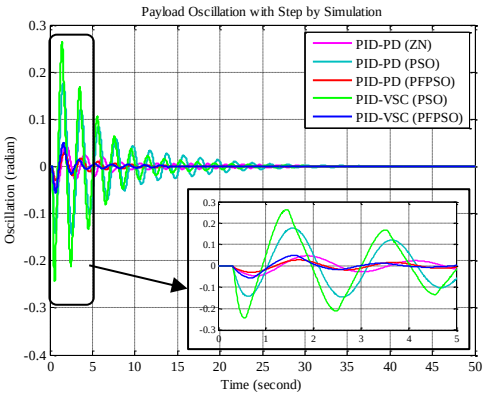

Figure 5 Response of payload oscillation.

Table 4 Performance in payload oscillation.

Tuning Methods	Performances	
	α_{max} (radian)	T_s (second)
PID-PD (ZN)	0.048	35.650
PID-PD (PSO)	0.177	35.310
PID-PD (PFPSO)	0.029	24.280
PID-VSC (PSO)	0.263	30.760
PID-VSC (PFPSO)	0.039	16.250

5. CONCLUSION

As conclusion, the simulation result of 3D INTECO GCS controlled by PID-VSC controller optimized by PFPSO show better performance in controlling the trolley position and minimizing the payload oscillation. In future work, robustness test can be examined in order to test the robustness of controller in GCS.

REFERENCES

[1] S.Y.S. Hussien, R. Ghazali, H.I. Jaafar and C.C. Soon, "Experimental analysis of 3D gantry crane system via optimal PID and PD controller by PSO", in *Proceedings of Mechanical Engineering Research Day*, 2016, pp. 66-68.

[2] H.I. Jaafar, S.Y.S. Hussien and R. Ghazali, "Optimal tuning of PID+PD controller by PFS for gantry crane system," in *10th Asian Control Conference (ASCC)*, 2015, pp. 1–6.

Validation of Radiation efficiency using Maidanik's Formula

K.H. Lim[1, 2], A. Putra[1, 2,*], R. Ramlan[1, 2]

[1)] Faculty of Mechanical Engineering, Universiti Teknikal Malaysia Melaka, Hang Tuah Jaya, 76100 Durian Tunggal, Melaka, Malaysia
[2)] Centre for Advanced Research on Energy, Universiti Teknikal Malaysia Melaka, Hang Tuah Jaya, 76100 Durian Tunggal, Melaka, Malaysia

[*]Corresponding e-mail: azma.putra@utem.edu.my

Keywords: Radiation efficiency; beam-stiffened; sound radiation

ABSTRACT – Beam-stiffened technique had been widely used in various industry. However, this may lead to undesired noise from the structure. This paper compares the radiation efficiency results calculated from Hybrid Mathematical Modelling with radiation efficiency results calculated from Maidanik's approximate formula. A good agreement can be observed at below and above coincidence frequency between the radiation results calculated from both models.

1. INTRODUCTION

Industry such as aerospace, ship hulls and cars, beam-stiffened technique can be seen applied to minimize the vibration of the structure, strengthen the overall structure or to prevent the structure from buckling. However, this technique may lead to cause undesirable noise. Many researchers have found that adding stiffener to the plate increases the radiation efficiency of the plate especially at mid-high frequency [1,2].

This paper compares the radiation efficiency calculated from proposed model known as Semi-analytical model with radiation efficiency results calculated from Maidanik's approximate formula. Maidanik's approximate formula had been used by several researchers to validate their mathematical modelling or modify it to use for different environment [3,4].

2. METHODOLOGY

2.1 Semi-analytical mathematical modeling

Radiation efficiency of a vibrating structure can be defined as the ratio of total acoustic power radiated over the spatially averaged mean squared velocity of the plate,

$$\sigma = \frac{W}{\rho c S \langle v^2 \rangle} \quad (1)$$

where W is the total acoustic power radiated, ρ is the density of the plate, c is the speed of sound and $\langle v^2 \rangle$ is mean squared velocity of the plate. To calculate the radiation efficiency of beam-stiffened plate, Semi-analytical Model developed by Putra.el.al is adopted in this paper.

Conceptually, this combines Finite Element method with analytical model. FE model is used to calculate the surface plate velocities results and then used it as input to calculate the radiated sound power through Rayleigh integral. The main advantage of using this model is that it can be apply to calculate sound radiation from complex structures. It helps to save time and effort from modelling the behavior of complex structure. The governing equation of this model can be refer in Putra et al. [5].

2.2 Maidanik's approximate formula.

Total sound power radiated W, from the panel given by Maidanik is

$$W = \sum_A \langle v_p^2 \rangle_A R_{rad}^x(A) + \sum_c \langle v_p^2 \rangle_c R_{rad}^y(C) + \sum_B \langle v_p^2 \rangle_B R_{rad}(B) \quad (2)$$

where $\langle v_p^2 \rangle$ is mean squared velocity of the panel is, R_{rad} is radiation resistance of the panel, A, B, and C is the x-edge modes, corner modes and y-edge modes of the panel. Below the coincidence frequency, by assuming equal modal energy the mean velocity of the panel can written as

$$\langle v_p^2 \rangle_A \approx \langle v_p^2 \rangle_B \approx \langle v_p^2 \rangle_C \approx \langle v_p^2 \rangle_1 \quad (3)$$

Taken in account of all the assumption mentioned yield approximate formula given as

$$\sigma = \begin{cases} (\lambda_a \lambda_b / A_p) g_1 + (P_r \lambda_b / A_p) g_2, & f < f_c \\ 0.45\sqrt{\dfrac{P f_c}{c}}, & f = f_c \\ \left(1 - \dfrac{f_c}{f}\right)^{-1/2}, & f > f_c \end{cases} \quad (4)$$

where

$$g_1 = \begin{cases} (4/\pi^4)(1-2\alpha^2)/\alpha(1-\alpha^2)^{1/2}, & f < 1/2 f_c \\ 0, & f > 1/2 f_c \end{cases} \quad (5)$$

and

$$g_2 = (2\pi)^{-2} \frac{(1-\alpha^2)\ln[(1+\alpha)/(1-\alpha)] + 2\alpha}{(1-\alpha^2)^{3/2}} \quad (6)$$

where α is f / f_c, f_c is coincidence frequency, P is the perimeter of the plate, A_p is the area of the plate, P_r is the perimeter of the system λ_a and λ_b is wavelength of acoustic field and panel.

The second term in eq. 4 is adopted from [6] as the original term overestimate the radiation efficiency at exactly coincidence frequency. For more detail information regarding Maidanik approximate formula, one can refer to Xie et al. [6].

3. RADIATION EFFICIENCY OF UNSTIFFENED AND STIFFENED PLATE

Radiation efficiency of unstiffened plate, single-beam stiffened, and three-beams stiffened plate are calculated using Hybrid mathematical model to compared with radiation efficiency calculated from Maidanik's approximate formula. All three panels including the stiffeners are assigned with aluminum properties: Young modulus E , 7.1×10^{10} N/m^2 ,density ρ 2700 kg/m^3 and damping loss factor $\eta = 0.001$. The panels have dimension of $0.5\times0.6\times0.003$ m whereas each stiffeners has dimension of $0.02\times0.2\times0.5$ m. Figure 1 show the detail and configuration of the three panels.

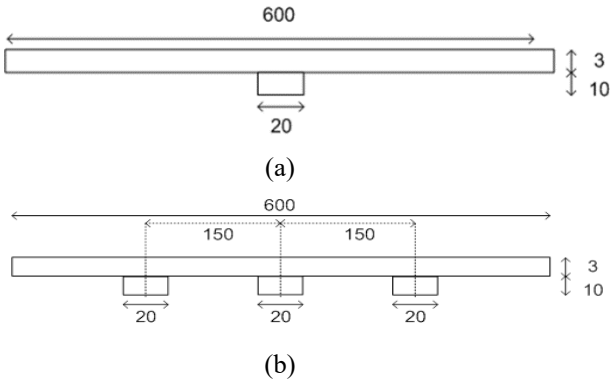

Figure 1 Dimension and configuration of (a) single-beam stiffened (b) three-beams stiffened plate in mm.

Figure 2 shows the radiation efficiency of unstiffened plate, single-beam stiffened plate and three-beams stiffened plate compared with Maidanik's formula. It can be observed that above the monopole region radiation efficiency result calculated from Hybrid mathematical method show good agreement with results calculated from Maidanik's formula.

This agree with Maidanik's findings that radiation efficiency is directly proportional with the total perimeter of the system and ribbing increase radiation efficiency of the plate. However, Maidanik's approximate formula is only limited to predict radiation efficiency for simply supported and very lightly damped plate. Disagreement between radiation efficiency results calculated from Maidanik's formula and semi-analytical model can be observed at low frequency. This is due to the low modal density at this frequency range where Maidanik's formula cannot be used to predict radiation efficiency result of the plate.

4. SUMMARY

Radiation efficiency of unstiffened, single-beam stiffened, and three-beams stiffened plate results calculated using hybrid mathematical model and Maidanik's approximate formula are presented. Comparing the results from both model show good agreement at frequency below and above coincidence frequency.

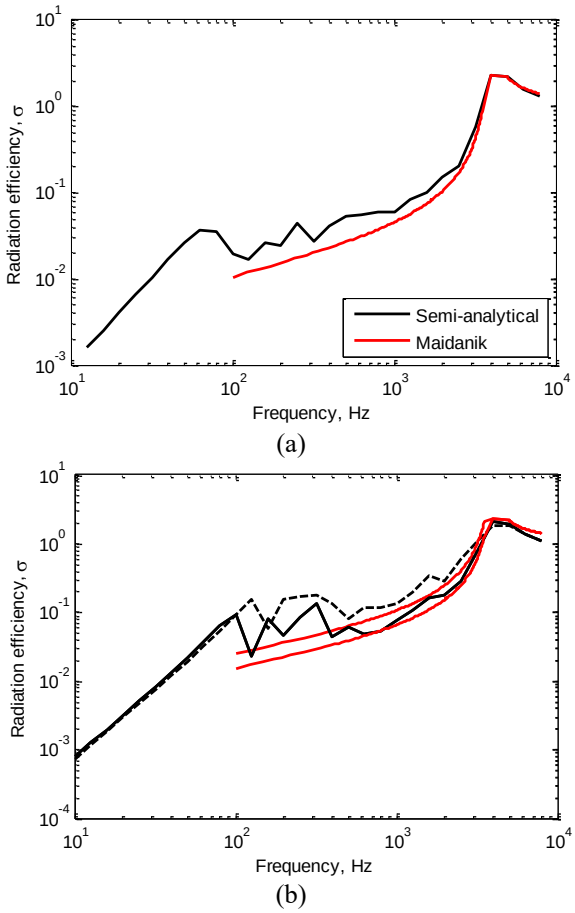

Figure 2 Comparison of radiation efficiency between semi-analytical model (black) and Maidanik's formula (red): (a) unstiffened (b) Stiffened plate: Single-beam (solid) and Three-beams (dash line).

REFERENCES

[1] G. Maidanik, "Response of ribbed panels to reverberant acoustic fields," *The Journal of the Acoustical Society of America*, vol. 34, no. 6, p. 809-826, 1962.

[2] A. Berry and J. Nicolas, "Structural acoustics and vibration behavior of complex panels," *Applied Acoustics*, vol. 43, no. 3, pp. 185-215, 1994.

[3] Z. Cheng, J. Fan, B. Wang and W. Tang, "Radiation efficiency of submerged rectangular plates," *Applied Acoustics*, vol. 73, no. 2, pp. 150-157, 2012.

[4] N. Hashimoto, "Measurement of sound radiation efficiency by the discrete calculation method," *Applied Acoustics*, vol. 62, no. 4, pp. 429-446, 2001.

[5] A. Putra, N. Shyafina, N. Muhammad, H. Bakri and N. Saari, "Development of hybrid semi-analytical and finite element analysis to calculate sound radiation from vibrating structure," *Advanced Materials Research*, vol. 845, pp. 71-75, 2013.

[6] G. Xie, D. Thompson and C. Jones, "The radiation efficiency of baffled plates and strips," *Journal of Sound and Vibration*, vol. 280, no. 1-2, pp. 181-209, 2005.

Effect of perforated plate on sound absorption of kenaf fibre

Z.Y. Lim[1], A. Putra[1,2,*], M.J.M. Nor[1,2], M.Y. Yaakob[3]

[1)] Faculty of Mechanical Engineering, Universiti Teknikal Malaysia Melaka, Hang Tuah Jaya, 76100 Durian Tunggal, Melaka, Malaysia
[2)] Centre for Advanced Research on Energy, Universiti Teknikal Malaysia Melaka, Hang Tuah Jaya, 76100 Durian Tunggal, Melaka, Malaysia
[3)] Faculty of Manufacturing Engineering, Universiti Teknikal Malaysia Melaka, Hang Tuah Jaya, 76100 Durian Tunggal, Melaka, Malaysia

[*]Corresponding e-mail: azma.putra@utem.edu.my

Keywords: Absorption coefficient; kenaf fibre; perforated plate

ABSTRACT – This paper presents the sound absorption coefficient performance of kenaf fibre with added perforated plates. The low frequency absorption is improved with the introduction of perforated plates sandwiched between the fibre layer and the air cavity. The drawback of such combination is the dropped performance in higher frequency. Mathematical models were used to simulate predicted sound absorption coefficient.

1. INTRODUCTION

Natural fibres were widely studied in recent years as alternative to synthetic sound absorber materials. The sound absorption coefficient of natural material such as coir fibre is being studied by adding and altering its configuration by adding air cavity and perforated plates [1]. Reed, as a non-fibrous natural material is also being investigated on its sound absorption with fabric added on the specimen, the performance is enhanced through this method [2]. Kenaf fibres was previously explored as multiple layer fibrous sound absorber by layering together with coir fiber [3], with kenaf fibre layered at first layer on the surface, the peak absorption appeared at lower frequency, conversely when kenaf fibre is layered as second layer, high frequency absorption is seen to be enhanced. The absorption performance of adding perforated plate in kenaf fibre is lacking, and hence this study explores the possibility of including perforated plate in kenaf fibre. Simulated result is also used to validate the feasibility of such combination.

2. METHODOLOGY

2.1 Specimens

The kenaf fibre specimen used in this study is industrial prepared kenaf fiber and the perforated plates used are made from aluminium plate with thickness of 1 mm. All the specimens are cut into circular shape with diameter of 33 mm as shown in Figure 1 in order to be fitted into the impedance tube for measurement. The drilled holes on the aluminium plate are of diameter of 0.5 mm and the perforation percentage is 1 %.

2.2 Experimental set up

The impedance tube method according to ISO 10534-2 [4] is employed to measure the normal incidence sound absorption coefficient of the specimens investigated. Figure 2 shows the experimental set up for the measurement. The specimen is fitted into the removable holder according to interested arrangement with the first layer refers to the immediate layer after the rigid backing.

(a) (b)

Figure 1 (a) kenaf fibre specimen and (b) perforated plates with 1% perforation.

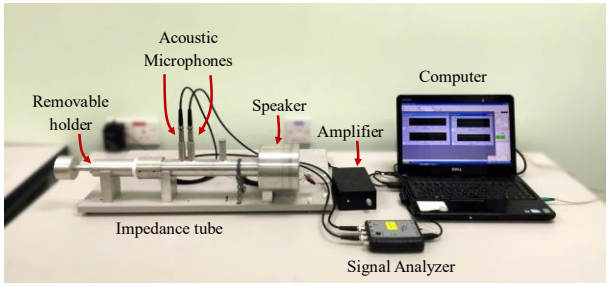

Figure 2 Experimental set up for measurement.

2.3 Mathematical models

The surface impedance air space layer is simulated through the characteristic impedance of air and propagation constant of air. Empirical model developed by Delany and Bazley [5] is employed to simulate the prediction absorption coefficient of kenaf fibre layer.

For the perforated plate, simulation is based on analytical solution provided by NorFlag™ Program.

3. RESULTS AND DISCUSSION

The addition of air cavity backing kenaf fibre is known to be able to improve the sound absorption coefficient of rigid backed kenaf fibre [6], this trend can be seen in Figure 3 when 10 mm of air gap is added to

the back of the 10 mm kenaf fibre. By introducing a perforated plate sandwiched between the air space and kenaf fibre, the low frequency range is observed to be significantly improved, having a peak recorded at around 1500 Hz. The drawback of such improvement is the drop of absorption coefficient at the high frequency region.

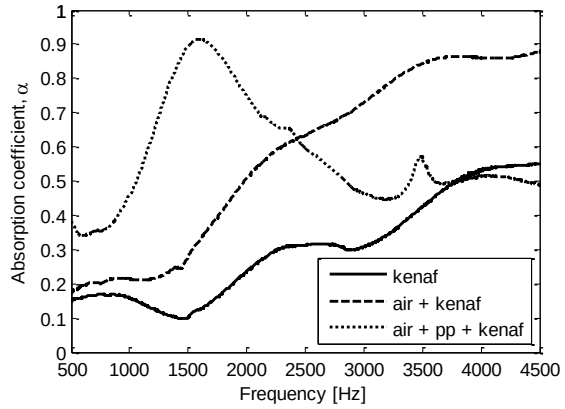

Figure 3 Sound absorption coefficient of 10 mm rigid backing kenaf fibre (──),
10 mm kenaf fibre backed with 10 mm air space (- - -), and 10 mm kenaf fibre backed with PP and 10 mm air space (·····).

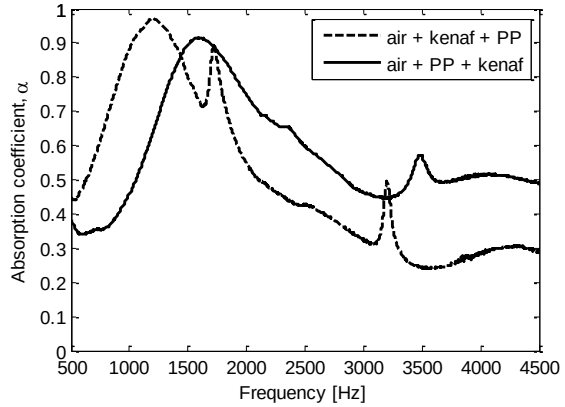

Figure 4 Sound absorption coefficient of multilayer specimen with 10 mm air space as first layer, 10 mm kenaf fibre as second and PP as third (- - -), and PP as second and kenaf fibre as third (──).

By altering the position of perforated plate and kenaf fibre to have the perforated plate facing the incidence sound, the peak absorption is seen to appear at lower frequency, as shown in Figure 4. However, the improvement is only observed below 1500 Hz, in frequency range higher than that, a poorer absorption is measured due to the nature of this configuration which tends to induce more resistance at low frequency.

The absorption coefficient of the specimen enhanced by air gap and PP is predicted, the comparison is as seen in Figure 5. Generally, the model employed to predict the absorption coefficient gives a promising estimation of the performance of the PP-enhanced material, the peak frequency is predicted well except a difference of 0.1 in absorption coefficient is estimated. The trend of the performance is well predicted. This agreement indicates that this model is suitable to be used in predicting the absorption coefficient of multilayer absorber involving PP.

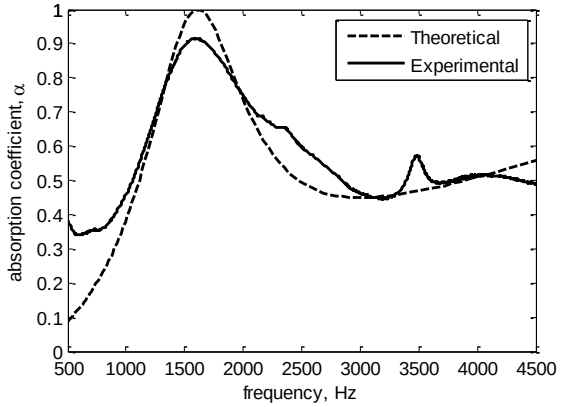

Figure 5 Measured (──) and predicted (- - -) sound absorption coefficient of 10 mm kenaf fibre backed with PP and 10 mm air space.

4. CONCLUSION

The introduction of perforated plate into kenaf fibre material is able to enhance the absorption performance only at low frequency region. With the perforated plate placed as the third layer following kenaf fibre as second and air space as the first layer, the peak absorption is improved and is shifted to low frequency, succumbing to the decreased absorption in high frequency region. The simulated result shows agreement with the measurement result, suggesting that the model can be used to predict the absorption of multilayer kenaf absorber involving perforated plate and air gap.

REFERENCES

[1] M. Ayub, M.H. Fouladi, M. Ghassem, M.J.M. Nor, H.S. Najafabadi, N. Amin, R. Zulkifli, "Analysis on multiple perforated plate sound absorber made of coir fiber," *International Journal of Acoustics and Vibration*, vol. 19, no. 3, pp. 203-211, 2014.

[2] F.A. Khair, A. Putra, M.J.M. Nor, M.Z. Selamat, "Enhancement on acoustical performance of reed 'Imperata Cylindrica'," in *Proceedings of Mechanical Engineering Research Day*, 2016, pp. 192-193.

[3] Z.Y. Lim, A. Putra, M.J.M. Nor and M.Y. Yaakob , "Natural coir fiber and kenaf fiber as multilayer sound absorber," in *Proceedings of Mechanical Engineering Research Day*, 2016, pp. 202-203.

[4] *Acoustics - Determination of sound absorption coefficient and impedance in impedance tubes - Part 2: Transfer-function method*, ISO 10534-2, 2001.

[5] M.E. Delany and E.N. Bazley, "Acosutical properties of fibrous absorbent materials," *Applied Acoustics*, vol. 3, no. 2, pp. 105-116, 1970.

[6] Z.Y. Lim, A. Putra, M.J.M. Nor and M.Y. Yaakob, "Preliminary study on sound absorption of natural kenaf fiber," in *Proceedings of Mechanical Engineering Research Day*, 2015, pp. 95-96.

Effect of tube length on the acoustical performance of plastic hollow tube sound absorber

F.A. Khair[1], A. Putra[1, 2,*], M.J.M. Nor[1,2], M.Z. Selamat[1, 2]

[1)] Faculty of Mechanical Engineering, Universiti Teknikal Malaysia Melaka, Hang Tuah Jaya, 76100 Durian Tunggal, Melaka, Malaysia
[2)] Centre for Advanced Research on Energy, Universiti Teknikal Malaysia Melaka, Hang Tuah Jaya, 76100 Durian Tunggal, Melaka, Malaysia

[*]Corresponding e-mail: azma.putra@utem.edu.my

Keywords: Hollow tube; analytical model; sound absorber

ABSTRACT – This paper discussed on utilizing the hollow tube structure as sound absorber since studies on non-fibrous type of sound absorber are still lacking. The effect of length of hollow tube structure towards sound absorption coefficient was studied and compared with both experimental and analytical method. The experiment was carried out using impedance tube method and analysis was accomplished through Zwikker and Kosten modeling approach. Both experiment and analytical model shows good agreement at peak frequency of absorption as increasing the length of the hollow tube.

1. INTRODUCTION

Sound absorber is known by its applications in reducing noise and improving sound intelligibility in building and industrial sector. Sound absorber absorbs the sound energy impinging on it through the conversion of heat and at the same time keeping the reflected sound waves at the surface as low as possible [1]. Sound absorber are classified into porous (fibrous type) and non-porous (resonator and membrane panel). There are numbers of empirical models on sound absorption have been developed for porous and non-porous materials [2-4]. However, studies on empirical models of hollow tube structure is still lacking. Thus, this paper presents the analysis on sound absorption of plastic hollow tube (lollipop sticks) by utilizing the empirical model that has been developed by Zwikker and Kosten for the case of pores with circular cross section. Result from analytical and experimental was compared for different length of hollow tube.

2. METHODOLOGY

The theoretical approach by Zwikker and Kosten [5] which using micro-structural approach that involves the propagation of wave inside the individual pores of circular cross section with consideration of viscous and thermal effects that leading to derivation of compression modulus K_i and complex density ρ_i. In this study, the hollow tube is from plastic material which is polypropylene (PP) of density 1000 kg/m^3. Figure 1 shows the arrangement of hollow tube and its minimal analysis model. From the minimal analysis model in Figure 1(b), a triangle prism is formed in between three neighbouring hollow tube. Taking the area of whole triangle as S_1, the area, S_3 and equivalent radius, R_{eq} of the curvy edges can be determined [6].

$$S_1 = \sqrt{3}R_o^{\,2} \tag{1}$$

$$S_2 = 1/2\,\pi R_i^{\,2} \tag{2}$$

$$S_3 = S_1 - 1/2\,\pi R_o^{\,2} \tag{3}$$

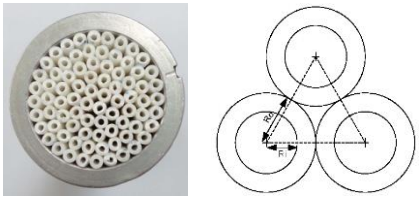

(a) (b)

Figure 1 (a) Hollow tube in axial arrangement, (b) minimal analysis model from three neighbouring hollow tube.

$$R_{eq} = \sqrt{S_3/\pi} \tag{4}$$

where R_i is the inner radius of hollow tube and R_o is the outer diameter of hollow tube. The open area ratio of hollow tube, $p_1$and in between gap p_2 is given as below,

$$p_1 = S_2/S_1 \tag{5}$$

$$p_2 = S_3/S_1 \tag{6}$$

The compression modulus, K_i and complex density ρ_i are derived as following.

$$\rho_i = \frac{\rho_0}{\left[1 - \frac{2}{\mu_{0i}\sqrt{-j}}\frac{J_1\left(\mu_{0i}\sqrt{-j}\right)}{J_0\left(\mu_{0i}\sqrt{-j}\right)}\right]} \tag{7}$$

$$K_i = \frac{\gamma P_0}{\left[1 + \frac{2}{B\mu_{0i}\sqrt{-j}}(\gamma - 1)\frac{J_1\left(B\mu_{0i}\sqrt{-j}\right)}{J_0\left(B\mu_{0i}\sqrt{-j}\right)}\right]} \tag{8}$$

where ρ_0 is the density of air, P_0 is the atmospheric pressure, γ=1.414 is the air specific heat ratio, B=0.86 is the Prandtl number for air, J_n is the Bessel function of order n, μ_{01} and μ_{02} are derived as below,

$$\mu_{01} = \sqrt{\omega\rho_0 R_i/\eta} \tag{9}$$

$$\mu_{02} = \sqrt{\omega\rho_0 R_{eq}/\eta} \tag{10}$$

The surface acoustic impedance for single tube, Z_1 and

gap in between tube, Z_2 is given by

$$Z_i = \sqrt{K_i \rho_i}\ \coth\left(j\omega l\sqrt{\rho_i / K_i}\right) \quad (11)$$

The hollow tube and the gap in between tube are considered in parallel arrangement, hence surface acoustic impedance expressed as below [6]

$$Z = \left(Z_1 / p_1 \cdot Z_2 / p_2\right) / \left(Z_1 / p_1 + Z_2 / p_2\right) \quad (12)$$

Hence, the absorption coefficient can be obtained as below

$$\alpha = 1 - \left|\frac{Z - \rho_0 c_0}{Z + \rho_0 c_0}\right|^2 \quad (13)$$

3. EXPERIMENT AND THEORETICAL RESULTS

Figure 2 shows the comparison of absorption coefficient obtained from experimental and theoretical of hollow tube for different length. Both results of experimental and theoretical shows good agreement especially at the peak absorption frequencies as the length of hollow tube increased. It is interesting to note that as the length of the hollow tube increase to 6 cm, both experimental and theoretical results shows second peak of absorption at high frequency with absorption coefficient almost unity. It shows that the sound absorption is mainly achieved by the hollow tube and gaps in between the hollow tube.

There is some difference in magnitude of absorption coefficient at before and after the peak absorption which is probably due to inconsistent result on equivalent radius of the curvy edge at the gap in between the hollow tube between actual arrangement and from minimal model as can be seen in Figure 1.

4. CONCLUSION

Overall, increasing length of hollow tube shows improvement in absorption coefficient at low and high frequency. Good agreement between analytical and experimental results are observed especially at peak absorption frequency.

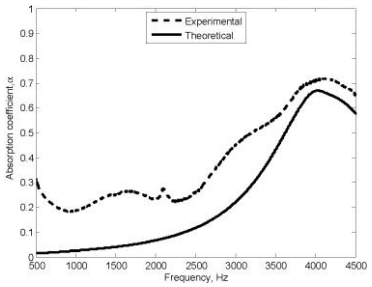

(a)

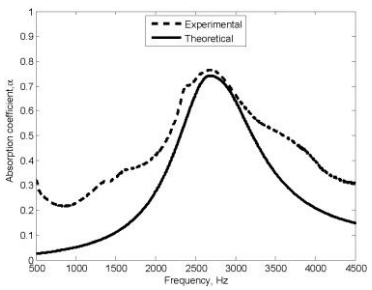

(b)

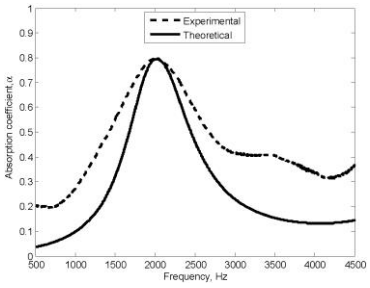

(c)

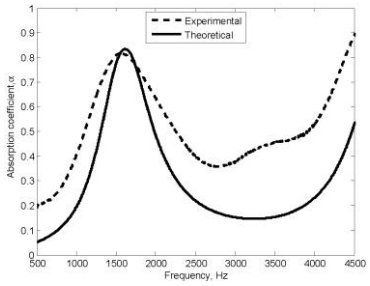

(d)

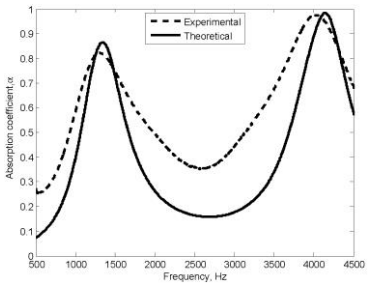

(e)

Figure 2 Comparison on measurement and theoretical result of hollow tube for different length: (a) 2 cm, (b) 3 cm, (c) 4 cm, (d) 5 cm and (e) 6 cm.

REFERENCES

[1] I.L. V'er, L.L Beranek, Noise and vibration control engineering: principles and applications, volume 966, 2nd ed. John Wiley & Sons; 2006.

[2] M.E. Delany and E.N. Bazely, "Acoustical properties of fibrous absorbent materials," *Applied Acoustics*, vol. 3, pp 105-116, 1970.

[3] D.Y. Maa, "Theory and design of microperforated panel sound-absorbing constructions," *Scientia Sinica*, vol. 18, no. 1, pp. 55-71, 1975.

[4] K. Sakagami, M. Kiyama, M. Morimoto and D. Takahashi, "Sound absorption of a cavity-backed membrane: a step towards design method for membrance-type absorber," *Applied Acoustics*, vol. 49, no. 3, pp 237-247, 1996.

[5] C. Zwikker and C.W. Kosten. *Sound absorbing materials*, Elsevier, New York; 1949.

[6] X. Hai, L. Yadong, Y. Jun and C. Xiaobin, "Acoustical characteristics of the sound absorption structure with densely arrayed capillary tube bundles," in *Proceedings of 23rd International Congress on Sound & Vibration*, 2015, pp. 1-7.

Sound absorption performance of suspended fabric

M.H. Jamil[1], A. Putra[1,2,*], M.J.M. Nor[1,2], K.H. Or[1], Z.Y. Lim[1]

[1)] Faculty of Mechanical Engineering, Universiti Teknikal Malaysia Melaka, Hang Tuah Jaya, 76100 Durian Tunggal, Melaka, Malaysia
[2)] Centre for Advanced Research on Energy, Universiti Teknikal Malaysia Melaka, Hang Tuah Jaya, 76100 Durian Tunggal, Melaka, Malaysia

[*]Corresponding e-mail: azma.putra@utem.edu.my

Keywords: Acoustic textile; cotton fabric; sound absorption coefficient

ABSTRACT – The sound absorption properties of materials are important not only for noise reduction, but also important for controlling reverberation time for speech intelligibility in a room. Nowadays, textile materials from the industry are studied to investigate its sound absorption performance. This research examines the acoustic performance of fabrics by the means of sound absorption coefficient. The test sample used is cotton fabric. The experimental measurement is conducted by using the impedance tube method. The results showed that 3 layers of fabric with 20 mm air gap thickness gives the best performance of sound absorption coefficient among the samples tested. It is found that the higher distance of gap between fabrics showed good absorption performance.

1. INTRODUCTION

Materials that reduce the energy of the sound waves by the phenomenon of absorption are called sound absorptive materials. These materials are commonly used to reduce the amplitude of the reflected waves of sound. Nowadays, the increasing request for quietness in building and auditoriums has inspired the use and development of better quality of sound absorptive material [1]. Among the acoustic absorptive materials, porous material is widely used and numerous achievements have been made in recent years [2]. Textile materials such as nonwoven, woven and knitted fabrics are porous materials and it has great ability for sound absorption application. Acoustical properties of textiles can be characterised in three categories, which are absorption, propagation and scattering. These acoustical properties can be expressed by flow resistance, transmission loss, absorption coefficient and scattering coefficient [3]. Putra et al. [4] conducted the experiment on sugarcane fibres and they found out that three layers of woven cloth absorber possess comparable sound absorption performance as the sugarcane fibres at the same thickness. Good sound absorption was achieved between frequencies of 1.2 to 4.5 kHz. Rwawiire et al. [5] studied on cellulose nonwoven natural fabric, namely *Antiaris toxicaria* (AT) barkcloth fabrics which can be found on the ceilings of vehicles. A small air gap of 15 mm between two AT layers significantly increased the sound absorption coefficient to a peak of 0.78 above 4 kHz. This paper discusses the acoustic performance of solely cotton fabrics with difference layers and distance, which according to the author's knowledge has not been investigated by other researchers.

2. METHODOLOGY

The cotton fabrics were cut into 33 mm diameter as shown in Figure 1 to fit into a sample holder of impedance tube for measurement. Experimental works were carried out with different numbers of fabric layer, such as single layer, 2 layers and 3 layers. Application of air gap was applied behind the sample to obtain a good measurement of the sound absorption coefficient.

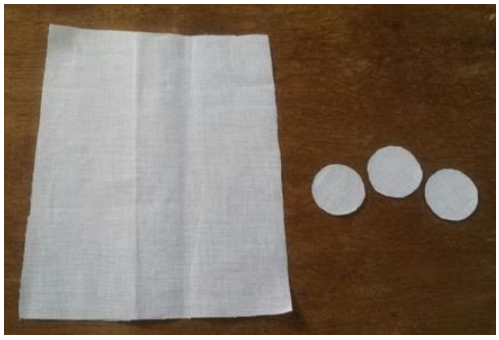

Figure 1 The cotton fabrics which had been cut into circular shape to be tested in the impedance tube testing.

The measurement of the sound absorption coefficient, α was conducted by using the impedance tube according to ISO 10534-2 [6]. Figure 2 shows the experimental setup that had been carried out. The sample was placed inside the sample holder tube located at one end of the impedance tube. The other end was the location of the loudspeaker. The loudspeaker was used as the source of white noise which was generated from the Audacity software and was then fed into the tube. Two acoustic microphones were assembled together with the preamplifier each and were located between the loudspeaker and the sample to record the built up sound pressure inside the impedance tube. RT Pro Photon+ analyser was used as the data acquisition system in this experiment. The white noise which generated from the loudspeaker was fed into the impedance tube for 10 minutes prior to the measurement to allow the temperature within the impedance tube to stabilise. 60 seconds of measuring time were used to obtain the sound absorption coefficient. The frequencies used in this experimental work are valid between the ranges of 500 Hz to 4.5 kHz.

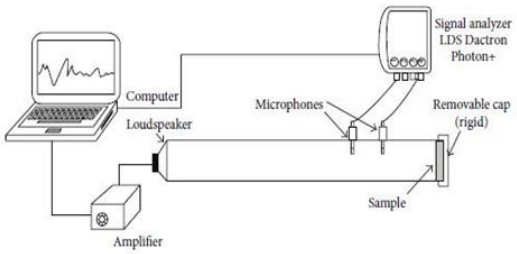

Figure 2 Experimental setup for the measurement of sound absorption coefficient.

3. RESULTS AND DISCUSSION

Figure 3 shows the absorption coefficient for samples with different layer of fabrics, but having the same air gap thickness of 10 mm. At the same air gap of 10 mm, 2 layers and 3-layer fabric showed good absorption coefficient (α) where $\alpha > 0.5$ above frequency of 2900 Hz and 1600 Hz respectively. It can be seen that increases the number of layers of the fabric improves the sound absorption coefficient significantly. This is due to the higher flow resistivity for additional layers of the fabric which allows more sound waves to be absorbed.

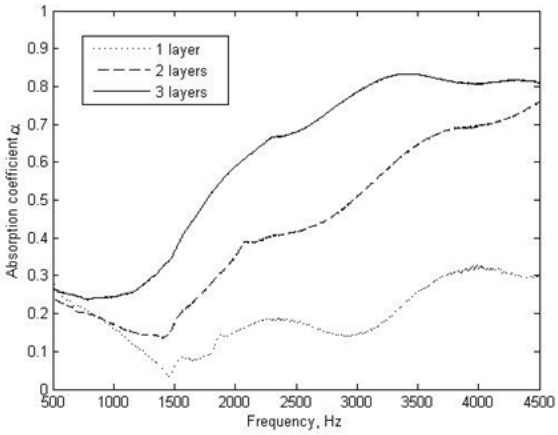

Figure 3 Sound absorption performance of fabric with different number of layers, but having the same 10 mm air gap thickness.

The effect of air gap can be seen in Figure 4, which the air gap thickness has been increased to 20 mm. It is shown that the increases of air gap thickness enhance the sound absorption coefficient and shifts the peak of the absorption coefficient to the lower frequency region. As a comparison, 3 layers of fabric in Figure 3 reached the peak of more than 0.8 at 3.4 kHz, has shifted to lower frequency at 1.6 kHz in Figure 4. For the 3 layers of fabric in Figure 4, improvement in the lower frequency region was compromised with degradation of the absorption coefficient at higher frequency region. However, the absorption coefficient still shown value of more than 0.5, which the reduction can still be acceptable.

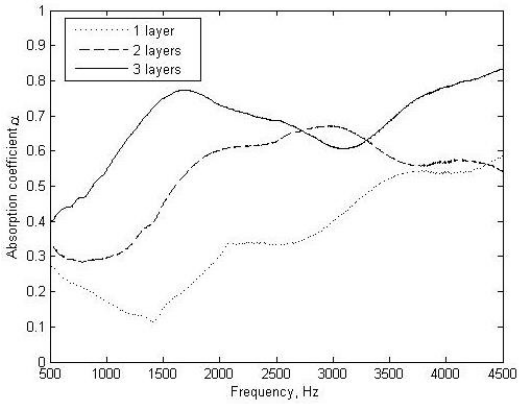

Figure 4 Sound absorption performance of fabric with different number of layers, but having the same 20 mm air gap thickness.

4. CONCLUSIONS

The cotton fabrics, which can be used for decoration purposes are found to be a good absorber. Increment of fabric layers showed the increasing of the sound absorption coefficient. The application of air gap improves the peak of sound absorption coefficient and shifts the curve to lower frequency region. The fabrics with 10 mm air gap thickness with 3 layers of fabric can reach absorption coefficient of 0.8 in average above 3 kHz. By doubling the air gap thickness to 20 mm, the improvement of absorption coefficient at all layers can be seen with $\alpha > 0.5$ cover wider frequency bandwidth.

ACKNOWLEDGEMENT

This research was supported by grant no.: PRGS/1/2014/SS07/FKM/02/T00005.

REFERENCES

[1] F. Shahani, P. Soltani and M. Zarrebini, "The analysis of acoustic characteristics and sound absorption coefficient of needle punched nonwoven fabrics," *Journal of Engineered Fabrics and Fibers*, vol. 9, no. 2, pp. 84-92, 2014.

[2] H.F. Xiang, D. Wang, H.C. Liua, N. Zhao and J. Xu, "Investigation on sound absorption properties of kapok fibers," *Chinese Journal of Polymer Science,* vol. 31, no.3, pp. 521-529, 2013.

[3] R. Nayak and R. Padhye, "Acoustic Textiles: An introduction," in *Acoustic Textiles*, Singapore: Springer; 2016, pp. 1-32.

[4] A. Putra, Y. Abdullah, H. Efendy, W.M.F.W. Mohamad, M.R. Ayob and M.S. Py, "Utilizing sugarcane wasted fibers as a sustainable acoustic absorber," *Procedia Engineering*, vol. 53, no. 1, pp. 632-638, 2013.

[5] S. Rwawiire, B. Tomkova, J. Militky, L. Hes and B.M. Kale, "Acoustic and thermal properties of a cellulose nonwoven natural fabric (barkcloth)," *Applied Acoustics,* vol. 116, pp. 177-183, 2017.

[6] Acoustics - Determination of sound absorption coefficient and impedance tubes - Part 2: Transfer-function method, ISO 10534-2, 2001.

Acoustic characteristic of pineapple leaf fibre

M.H. Hassan[1], A. Putra[1,2,*], M.Z. Selamat[1,2], K.H. Or[1,2], A.R. Dullah[1,2]

[1)] Faculty of Mechanical Engineering, Universiti Teknikal Malaysia Melaka, Hang Tuah Jaya, 76100 Durian Tunggal, Melaka, Malaysia
[2)] Centre for Advanced Research on Energy, Universiti Teknikal Malaysia Melaka, Hang Tuah Jaya, 76100 Durian Tunggal, Melaka, Malaysia

[*]Corresponding e-mail: azma.putra@utem.edu.my

Keywords: Natural fibre; pineapple leaf fibre; sound absorption coefficient

ABSTRACT – Synthetic materials are commonly used in building industry as acoustic absorber. However, the production of synthetic material can contribute to environmental problem such as pollutions and global warming. Problems arose have encouraged the researchers to find alternative materials to replace synthetic acoustic absorber. This paper discusses the sound absorption of pineapple leaf fiber as an acoustic absorber. Samples of acoustic absorber using PALF are fabricated with different masses and thicknesses. The effect of sample mass, thickness and air gap are studied through impedance tube method to obtain the sound absorption coefficient. PALF is found to show good sound absorption coefficient.

1. INTRODUCTION

Undesirable and harmful noise gives serious effects to the surrounding environment and also to human health. According to World Health Organization (WHO), they estimated that 10% of the population are exposed to the noise level that can cause hearing problem [1]. Traditionally, absorbent materials are made of synthetic materials such as glass wool and foam glass. These synthetic materials are found to be not only harmful to human health, but also cause pollutions and global warming [2]. Thus, researchers have changed their focus into 'green' materials as the alternative to the synthetic materials. Putra et al. [3] performed an experimental investigation on sound absorption of paddy fibre. Researcher found out that 3 grams and 20 mm thick of paddy fibres demonstrated comparable sound absorption coefficient with synthetic glass wool at the same thickness. Lim et al. [4] studied the sound absorption using multilayer of natural coir and kenaf fibres. The addition of kenaf fibre into coir fibre sample is found to significantly enhance the sound absorption as compared to sample consists of solely coir fibres. Or et al. [5] measured the sound absorption coefficient of oil palm empty fruit bunch fibres. Researcher noted that samples with thicknesses of 40 mm and 50 mm which having a density of 292 kg/m^3 showed good sound absorption performance with sound absorption coefficient of 0.9 in average above 1 kHz. Pineapple leaf is a biodegradable material and usually ends as waste material. This paper discusses the acoustic performance of raw Pineapple Leaf Fibre (PALF), which according to the author's knowledge has not been investigated by other researchers.

2. METHODOLOGY

Figure 1 shows the pineapple leaves and the extracted PALF. The PALF were extracted by using a machine called *Mesin Pemacah Daun Nen*as. The leaves were fed through the feed roller and passed through the leaf scratching roller by 'grind' process. The PALF was then obtained by pulling off the leaf from the machine. According to Das et al. [6], a pineapple leaf contains 2.5 to 3.5% of fibre from its total weight. The extracted PALF were treated with alkaline solution in order to remove the chemical constituents, dirt and any particle.

(a) (b) (c)

Figure 1 (a) Pineapple leave before the extraction process, (b) pineapple leaves after the extraction process and (c) pineapple leaf fibres after alkaline treatment.

The PALF were weighted for 1 gram and 2 grams, and were then fitted into 33 mm diameter aluminium web casing for sample preparation. The thickness of the PALF samples was the thickness of the web casing as shown in Figure 2.

(a) (b)

Figure 2 Pineapple leaf fibre samples: (a) 1 gram and 10 mm thick, and (b) 2 grams and 20 mm thick.

The measurement of sound absorption coefficient, α was conducted by using an impedance tube (see Figure 3) based on ISO 10534-2 [7]. The sample of PALF was fitted into the sample holder and was located at one end of the impedance tube. The other end of the tube was the location of a loudspeaker. Audacity 1.3 Beta software generated the white noise and supplied it into the tube through the loudspeaker. Two 1/2" pre-polarised acoustical microphones and 1/2" CCP pre-amplifier were located between the sample and the loudspeaker to record the built-up sound pressure. The frequency range of this experiment is valid between 500 to 4500 Hz according to ISO 10534-2.

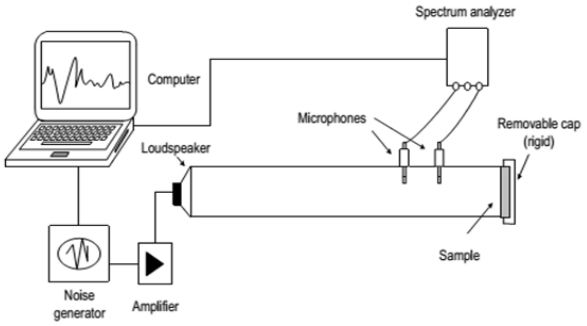

Figure 3 Experimental setup for the measurement of sound absorption coefficient.

3. RESULTS AND DISCUSSION

Figure 4 shows the comparison of PALF with different masses and different thicknesses, but having the same density. From the graph, it shows that increases of thickness and mass significantly improves the absorption coefficient and shifts the peak of the absorption coefficient to the lower frequency region. Both of the samples show good sound absorption property above 2.3 kHz where $\alpha > 0.5$. Increasing the mass of the sample contributes to increases of the flow resistivity, which increases the difficulty of the path for the sound waves to flow through the fibres. At the same density, thicker sample contains more fibres and thus, allows more sound waves to be absorbed through the surface friction.

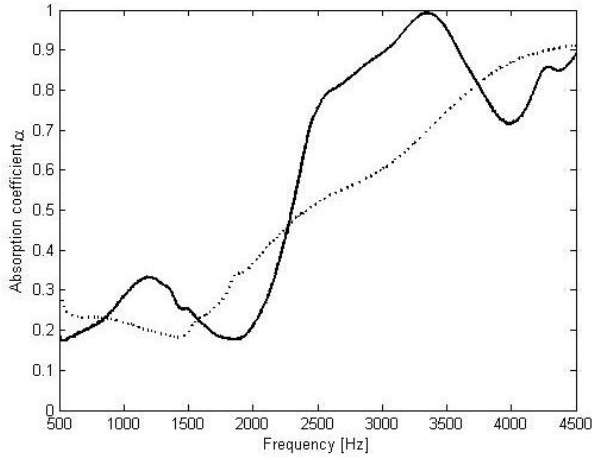

Figure 4 PALF with two different masses and thicknesses: 10 mm, 1 gram (dotted line) and 20 mm, 2 grams (solid line).

Figure 5 shows the effect of air gap on the sound absorption performance of PALF. Application of air gap behind the sample has shown enhancement of the absorption coefficient at lower frequencies. The peak of the absorption coefficient curve has shifted to the left or lower frequency region. However, improvement of absorption coefficient at lower frequencies accompanied with slightly reduced of absorption coefficient at higher frequencies.

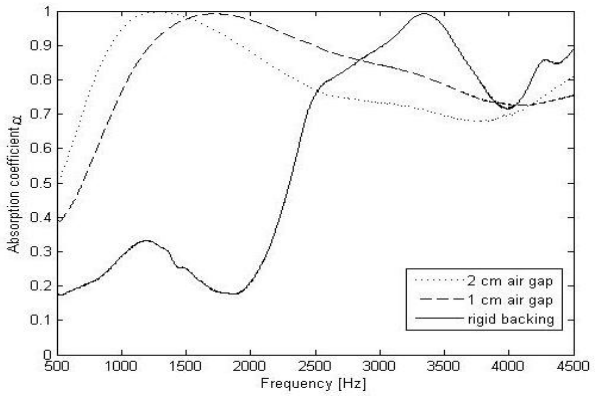

Figure 5 Sound absorption performance of 2 grams and 20 mm thick PALF sample with different air gaps.

4. CONCLUSIONS

The pineapple leaf fibres are found to be good sound absorber. The increment of mass and thickness yields higher peak of absorption coefficient and the peak of absorption coefficient shifts to lower frequencies. Application of air gap enhances the sound absorption coefficient, especially at lower frequency region. As a conclusion, samples with and without air gap show peak value $\alpha > 0.9$.

ACKNOWLEDGEMENT

This research was supported by grant no. PRGS/1/2014/SS07/FKM/02/T00005.

REFERENCES

[1] Science Communication Unit, University of the West of England (UWE), Bristol (2015, January), *Thematic issue: Noise impacts on health* [Online]. Available: http://ec.europa.eu/environment/integration/research/newsalert/pdf/47si.pdf

[2] F. Asdrubali, "Survey on the Acoustical Properties of New Sustainable Materials for Noise Control," in *Proceedings of the Euronoise*, Tampere, Finland, 2006, pp. 1-10.

[3] A. Putra, Y. Abdullah, H. Efendy, W.M.F.W Mohamad and N.L. Salleh, "Biomass from paddy waste fibers as sustainable acoustic material," *Advances in Acoustics and Vibration,* vol. 2013, pp. 1-7, 2013.

[4] Z.Y. Lim, A. Putra, M.J.M. Nor, N. Muhammad and M.Y. Yaakob, "Sound absorption of multilayer natural coir and kenaf fibers," in *The 23rd International Congress of Sound and Vibration*, 2016, pp. 1-7.

[5] K.H. Or, A. Putra and M.Z. Selamat, “Oil palm empty fruit bunch fibers as sustainable acoustic material,” *Applied Acoustics,* vol. 119, pp. 9-16, 2017.

[6] P.K. Das, D. Nag, S. Debnath and L.K. Nayak, “Machinery for extraction and traditional spinning of plant fibres,” *Indian Journal of Traditional Knowledge,* vol. 9, no. 2, pp. 386-393, 2010.

[7] *Acoustics - Determination of sound absorption coefficient and impedance in impedance tubes - Part 2: Transfer-function method*, ISO 10534-2, 2001.

Improvement of cutting force using ultrasonic vibration for machining mold and die materials

R. Azlan[1,2], R. Izamshah[1,*], M. Hadzley[1], M.S. Kasim[1], M. Arfauz[1], M. Akmal[1]

[1)] Faculty of Manufacturing Engineering, Universiti Teknikal Malaysia Melaka, Hang Tuah Jaya, 76100 Durian Tunggal, Melaka, Malaysia.
[2)] Department of Mechanical Engineering, Politeknik Melaka, Balai Panjang, Plaza Pandan Malim, 75250 Melaka, Malaysia.

[*]Corresponding e-mail: izamshah@utem.edu.my

Keywords: Ultrasonic assisted machining; surface roughness; hardened steel

ABSTRACT – Conventional machining of mold and die materials poses several challenges due to the high strength of these materials that generate high cutting force which affect the machining performances. To solve this issue, this paper introduced an ultrasonic vibration frequency apply on the conventional machine tool aim to reduce the magnitude of cutting force. Set of experimental work with different machining parameters namely cutting speed feed rate and axial depth of cut were perform to evaluate the effectiveness of the technique. From the conducted experimental work, it shows that the present of ultrasonic vibration reduced the magnitude of the cutting force up to 86% reduction in trust force, Fz compared to the conventional machining process with the same cutting condition. The present of the ultrasonic vibration creates an equivalent of a torsional peck cycle in which the cutting edge practically sawing through the materials as it goes creating a repeated relaxing engagement with the cut resulting in lower friction and cutting force.

1. INTRODUCTION

Most of the material used for mold and die material are made from hardened steel (~40-60 HRc) which are categorized as difficult to cut material due to its superior hardness. The cutting process of this material involves the generation of high cutting force which lessen the machining performances such as high machining temperature and rapid tool wear.

Rotary ultrasonic machining is a non-conventional machining process that combined between rotary end milling action and ultrasonic vibration movement [1-3]. A rotating horn with a piezo material actuated the cutting tool and vibrates ultrasonically with frequency 20-27 kHz in axial direction and feed downwards to the work piece [3].

By incorporating the ultrasonic frequency to the rotating cutting tool, the vibration oscillation amplitude of the tool are altered that had imposed a static pressure on the workpiece surface grains, in which the workpiece surface is hammered into, and finally a peening surface is produced that improved the surface finish by reducing the peak height produced from the milling cutter [4-5]. In addition, the transmitted oscillating vibration also reduced the contact pressure between the cutting tool and the workpiece, thus reducing the machining force and temperature that consequently prolongs the cutting tool life.

The aim of this study was to evaluate the effectiveness of incorporating the ultrasonic vibration to the rotating cutting tool in reducing the magnitude of cutting forces on different parameters namely cutting speed, feed rate and machining depth on hardened AISI D2 material.

2. METHODOLOGY

The material used for the experiment was AISI D2 tool steel block with the hardness of 51 ± 2 HRc and dimension of 120 X 100 X 20 mm (l x w x h). Slot milling test are perform using a 3 axis HAAS VF-1 CNC milling machine. A BT40 ultrasonic tool holder with a frequency of 23.83 kHz and amplitude of 2 μm was used with a 2 flutes and 6 mm diameter carbide flat end mill attached at the end of the holder. Details of the experiment setup are shown in Figure 1. All machining experiment were performed in dry cutting condition without any lubricants. The measurement of cutting forces (Fx, Fy, Fz) were done using Kistler 3 component Dynamometer type 5233A. Totals of 16 runs were perform at different level setting between parameter to investigate the correlation between the presence ultrasonic vibration and machining parameter with the magnitude of cutting forces.

3. RESULTS AND DISCUSSION

Table 1 shows the effect of machining parameters on cutting force magnitude with the presence of ultrasonic vibration and conventional machining. From the result, it clearly shows the reduction in force magnitudes with the presence of ultrasonic vibration for all the runs. Apart from that, it shows that feed rate was the main factor that affected the generated cutting force for both cases. Increasing in feed rate value causing to increase the cutting force magnitude. The highest thrust force (Fz) magnitude was observed for Run 3 with a value of 58.9 N without the presence of the ultrasonic vibration compared with cutting force produced with the presence of ultrasonic vibration been 25.6 N (run 4) on the same cutting condition (*Vc* = 0.6 m/min, *feed* = 100 mm/min, *DoC* = 12 μm).

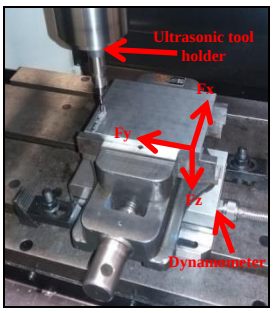

Figure 1 Experimental setup.

Table 1 Experimental results.

Run	*Vc* m/min	*feed* mm/min	*DoC* mm	Ultrasonic	Fx	Fy	Fz
					Newton (N)		
1	0.6	100	10	Off	5.19	1.37	40.28
2				On	1.07	0.31	19.23
% Reduction of Cutting Force (Fx, Fy, Fz)					79.4 %	77.4 %	52.3 %
3	0.6	100	12	Off	3.82	0.46	58.89
4				On	2.75	0.15	25.63
% Reduction of Cutting Force (Fx, Fy, Fz)					28.0 %	67.4 %	56.5 %
5	3	5	12	Off	1.68	0.77	25.33
6				On	0.61	0.15	3.66
% Reduction of Cutting Force (Fx, Fy, Fz)					63.7 %	80.5 %	85.6 %
7	3	100	10	Off	19.07	29.60	29.60
8				On	7.17	22.28	28.08
% Reduction of Cutting Force (Fx, Fy, Fz)					62.4 %	24.7 %	5.1 %
9	3	100	12	Off	24.11	17.09	20.75
10				On	1.68	4.58	19.23
% Reduction of Cutting Force (Fx, Fy, Fz)					93.0 %	73.2 %	7.3 %
11	0.6	5	10	Off	1.62	8.09	14.75
12				On	0.89	1.42	13.72
% Reduction of Cutting Force (Fx, Fy, Fz)					45.1 %	82.4 %	7.0 %
13	3	5	10	Off	2.87	4.86	17.14
14				On	2.35	2.43	16.96
% Reduction of Cutting Force (Fx, Fy, Fz)					18.1 %	50.0 %	1.1 %
15	0.6	5	12	Off	3.21	3.36	22.14
16				On	2.82	2.92	13.73
% Reduction of Cutting Force (Fx, Fy, Fz)					12.1 %	13.1 %	38.1 %

Figure 2-4 shows the comparison graph of cutting force for Fx, Fy and Fz respectively between conventional and rotary ultrasonic assisted milling for all the runs.

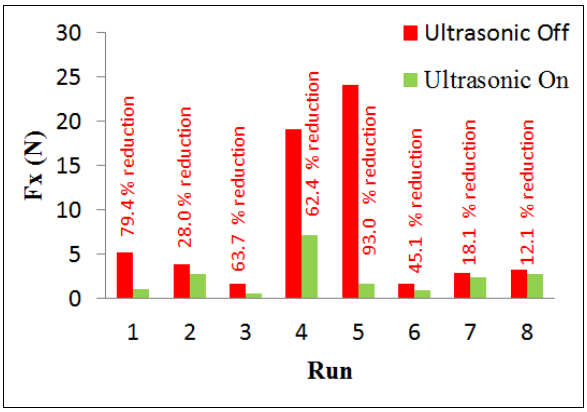

Figure 2 Magnitude of Fx between conventional and ultrasonic machining.

4. CONCLUSIONS

This study has shown on the effectiveness of applying the ultrasonic vibration technique for reducing the machining forces. The present of the ultrasonic vibration creates an equivalent of a torsional peck cycle in which the cutting edge practically sawing through the materials as it goes creating a repeated relaxing engagement with the cut resulting in lower friction and cutting force. From the conducted experimental work, it shows that the present of ultrasonic vibration reduced the magnitude of the cutting force up to 86% reduction in trust force, Fz compared to the conventional machining process with the same cutting condition.

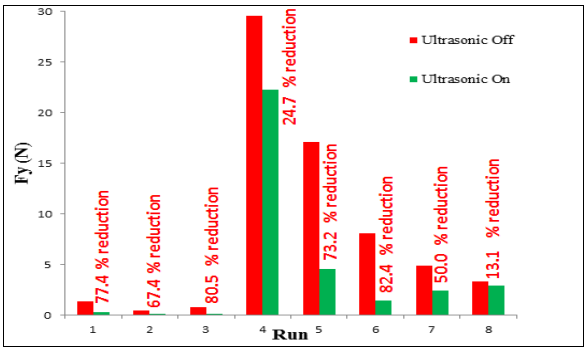

Figure 3 Magnitude of Fy between conventional and ultrasonic machining.

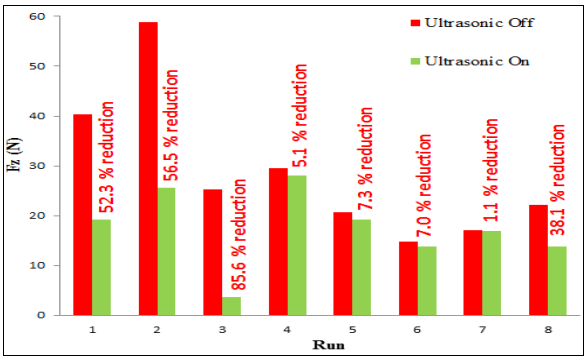

Figure 4 Magnitude of Fz between conventional and ultrasonic machining.

REFERENCES

[1] W. L. Cong, Z. J. Pei, N. Mohanty, E. Van Vleet and C. Treadwell, "Vibration amplitude in rotary ultrasonic machining: A novel measurement method and effects of process variables," *J. Manuf. Sci. Eng.*, vol. 133, no. 3, pp. 34501–34505, 2011.

[2] N. J. Churi, Z. J. Pei and C. Treadwell, "Rotary ultrasonic machining of titanium alloy (Ti-6Al-4V): effects of tool variables," *Int. J. Precis. Technol.*, vol. 1, no. 1, p. 85-96, 2007.

[3] Y. Ahmed, W. L. Cong, M. R. Stanco, Z. G. Xu, Z. J. Pei, C. Treadwell, Y. L. Zhu and Z. C. Li, "Rotary ultrasonic machining of alumina dental ceramics: A preliminary experimental study on surface and subsurface damages," *J. Manuf. Sci. Eng.*, vol. 134, no. 6, p. 64501-64505, 2012.

[4] R.Azlan, R.Izamshah, M.Hadzley, M.S. Kasim and M. Arfauz, "Experimental investigation of surface

roughness using ultrasonic assisted machining of hardened steel," in *Proceedings of Mechanical Engineering Research Day*, 2016, pp. 212–213.

[5] R.Azlan, R. Izamshah, M. Hadzley, M.S. Kasim and M. Arfauz, "Surface evaluation of rotary ultrasonic assisted machining technique," in *Adv. Process. Syst. Manuf. An Int. Conf. 2016*, 2016, pp. 11–12.

Comparison of sound absorption performance of aluminium and cardboard micro-perforated panel

K.H. Or[1,2], A. Putra[1,2,*], R.M. Dan[1,2], Z.Y. Lim[1,2]

[1)] Faculty of Mechanical Engineering, Universiti Teknikal Malaysia Melaka, Hang Tuah Jaya, 76100 Durian Tunggal, Melaka, Malaysia
[2)] Centre for Advanced Research on Energy, Universiti Teknikal Malaysia Melaka, Hang Tuah Jaya, 76100 Durian Tunggal, Melaka, Malaysia

[*]Corresponding e-mail: azma.putra@utem.edu.my

Keywords: Micro-perforated panel; cardboard; sound absorption coefficient

ABSTRACT – Blurry noise or echo can cause disturbance to human being, especially in big halls, classrooms, auditoriums, cinemas and offices. This paper discusses the application of aluminium and cardboard micro-perforated panels (MPP) as acoustic absorber. Samples of MPP with different materials and perforation ratios are fabricated. The effect of type of material, introduction of air gap behind the sample and perforation ratio on the sound absorption performance are investigated through impedance tube testing to obtain the sound absorption coefficient. Both the aluminium and cardboard MPP are found to be effective acoustic absorber, especially at lower frequencies.

1. INTRODUCTION

Noise can be defined as any perceived sound which is uncomfortable to the ear of the human being [1]. Blurry sound or echo, which is noise at low frequencies can decreases speech intelligibility especially in classrooms, auditoriums, cinemas, offices and working environment. Perforated panel (PP) or micro-perforated panel (MPP) is a type of acoustic absorber which is used to manage the reverberation at low frequency [2]. The absorption mechanism of PP or MPP occurs at the resonance frequency. Ayub et al. [3] summarised that in the application of 3 PPs into coir fibre and air gap layers, the higher porosity PP which faced the sound source will control the absorption at high frequencies, the medium porosity PP between the coir fibres will provide absorption at mid frequency range and the lower porosity of PP between the coir fibre and air gap layers will contribute to low frequencies absorption. Putra and Ismail [4] studied on the sound transmission loss of PP and MPP. They noted that the transmission loss increased as the perforation ratio decreased, increased as the hole diameter reduced for MPP and increased as the hole diameter increased for PP. This paper compares the sound absorption performance of aluminium and cardboard micro-perforated panels. According to the author's knowledge, the use of cardboard MPP for acoustic material has not been presented by other researchers.

2. METHODOLOGY

In this study, the cardboard and aluminium panels with the same thickness of 10 mm were cut into circular shape with diameter of 33 mm, which is the same diameter as the sample holder of an impedance tube. Holes with micron dimension were drilled on the circular panels to produce different perforation ratios, σ, i.e. 0.5% (22 microholes), 1.0% (44 microholes) and 1.5% (66 microholes). The samples are shown in Figure 1. The perforation ratio, σ is defined as the percentage of the total area of the microholes over the area of the 33 mm circular shape panel, given by $\sigma = (\sum A_m) / A_p \times 100\%$.

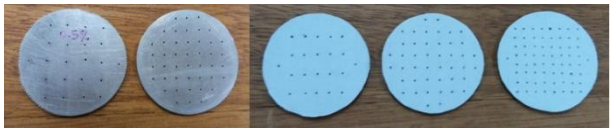

(a) (b) (c) (d) (e)

Figure 1 MPPs with different materials and perforation ratios: (a) aluminium with 0.5%, (b) aluminium with 1.0%, (c) cardboard with 0.5%, (d) cardboard with 1.0% and (e) cardboard with 1.5%.

The measurement of sound absorption coefficient was conducted by using the impedance tube testing following the ISO 10534-2 [5]. The measurement setup is shown in Figure 2. The sample was fitted tightly into the impedance tube and was located at one end of the tube. At the other end of the tube is the location of a loudspeaker, which produced white noise signal and fed the noise into the tube. Two 1/2" pre-polarised free field microphones (GRAS 40AE) with 1/2" CCP pre-amplifier (GRAS 26CA) were used to record the built-up sound pressure inside the tube. RT Pro Photon+ analyser was used as the data acquisition system to process the recorded signals. MATLAB software was then used to calculate the absorption coefficient. For this impedance tube testing, the results are valid between frequencies of 500 to 4500 Hz.

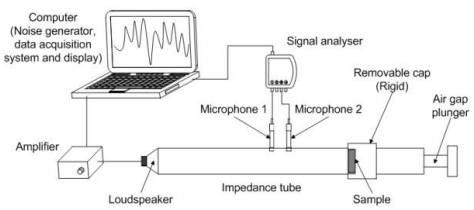

Figure 2 Experimental setup for the measurement of sound absorption coefficient by using impedance tube.

3. RESULTS AND DISCUSSION

Figure 3 shows sound absorption performance of MPP with air gap thickness of 20 mm. In terms of material, it can be seen that aluminium MPPs showed higher first peaks of the sound absorption coefficient curve in comparison to the cardboard MPPs. For the difference in perforation ratio, doubled the perforation ratio showed improvement on the peak of sound absorption coefficient. The interesting behaviour which differs between the aluminium and cardboard MPPs is the pointy peaks exhibited by the cardboard MPPs at 2 to 2.5 kHz. All the samples in Figure 3 showed poor sound absorption performance at high frequency region, i.e. 2.5 to 4.5 kHz.

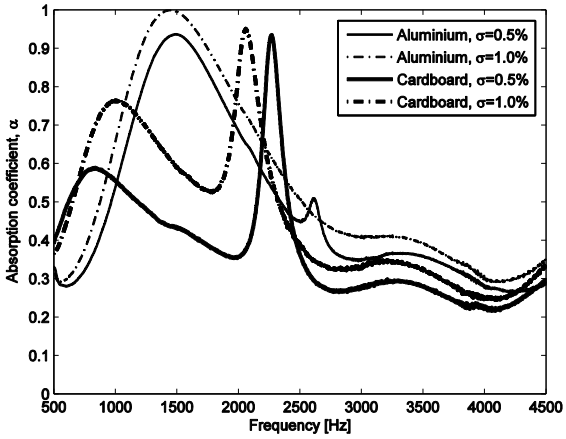

Figure 3 Sound absorption coefficient of MPPs with different materials and perforation ratios, but having the same air gap thickness of 20 mm.

Figure 4 illustrates sound absorption performance of MPP with bigger air gap thickness, i.e 45 mm. In comparison to Figure 3, the sound absorption coefficient curves in Figure 4 have shifted to the lower frequency region. Another obvious difference between Figure 3 and Figure 4 was the improvement of sound absorption performance at high frequency region, i.e. at 4.1 to 4.4 kHz, which can be seen by the pointy peaks at the end of the curves. Again, both cardboard MPPs presented pointy peaks at 2 to 2.5 kHz.

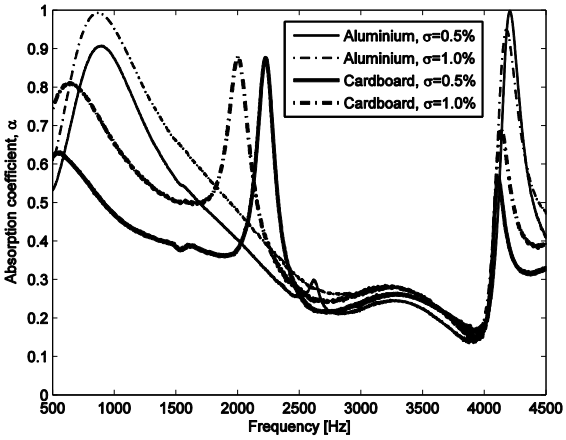

Figure 4 Sound absorption coefficient of MPPs with different materials and perforation ratios, but having the same air gap thickness of 45 mm.

Figure 5 compares sound absorption performance of cardboard MPPs with different perforation ratios and air gap thicknesses. For all the MPPs tested, the same behaviour is displayed at 2 to 2.5 kHz, where all pointy peaks showed sound absorption coefficient of more than 0.85. The pointy peaks occurred due to impinging sound waves which caused vibration mode on the rigid cardboard during experimental measurement. This behaviour results in more sound waves is attenuated.

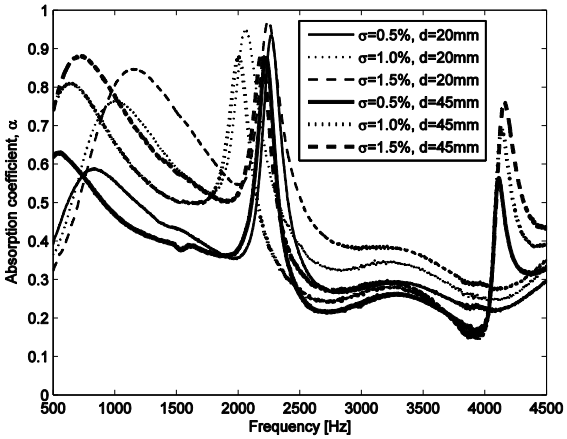

Figure 5 Sound absorption coefficient of cardboard MPPs with variation of perforation ratios and air gap thicknesses.

4. CONCLUSIONS

The aluminium and cardboard micro-perforated panels (MPP) shown good sound absorption performance at lower frequency region. The aluminium MPP presents higher peak of sound absorption coefficient curve as compared to cardboard MPP. Increment of perforation ratio increases the peak of the absorption coefficient curve. Extension of the air gap thickness from 20 mm to 45 mm has shown improvement of sound absorption performance where the curve shifts to the lower frequency region. The cardboard MPPs demonstrate interesting behaviour of sound absorption performance at 2 to 2.5 kHz, where pointy peaks of more than 0.85 appeared.

ACKNOWLEDGEMENT

This research was supported by grant no. FRGS/1/2014/TK01/FKM/03/F00210.

REFERENCES

[1] I.L. Ver and L.L. Beranek, *Noise and vibration control engineering: principles and applications*, 2nd ed. Wiley; 2006.

[2] F. Jacobsen, T. Poulsen, J.H. Rindel, A.C. Gade and M. Ohlrich, *Fundamentals of acoustics and noise control*, Department of Electrical Engineering, Technical University of Denmark; 2011.

[3] M. Ayub, M.H. Fouladi, M. Ghassem, M.J.M. Nor, H.S. Najafabadi, N. Amin and R. Zulkifli, "Analysis on multiple perforated plate sound

absorber made of coir fiber," *International Journal of Acoustics and Vibration*, vol. 19, no. 3, pp. 203-211, 2014.

[4] A. Putra and A.Y. Ismail, "Normal incidence of sound transmission loss from perforated plates with micro and macro size holes," *Advances in Acoustics and Vibration*, vol. 2014, pp. 1-12, 2014.

[5] *Acoustics - Determination of sound absorption coefficient and impedance in impedance tubes - Part 2: Transfer-function method*, ISO 10534-2, 2001.

Preliminary study on sound absorption coefficient of kapok fiber

Y.H. Abdullah[1], A. Putra[1,2,*], M.J.M. Nor[1,2], Z.Y. Lim[1], R.M. Dan[1,2]

[1)] Faculty of Mechanical Engineering, Universiti Teknikal Malaysia Melaka, Hang Tuah Jaya, 76100 Durian Tunggal, Melaka, Malaysia
[2)] Centre for Advanced Research on Energy, Universiti Teknikal Malaysia Melaka, Hang Tuah Jaya, 76100 Durian Tunggal, Melaka, Malaysia

[*]Corresponding e-mail: azma.putra@utem.edu.my

Keywords: Sound absorber; kapok fiber; absorption coefficient

ABSTRACT – In industry, the utilization of the synthetic materials as sound absorber are still ongoing even though these non-biodegradable materials do not only cause pollution to the environment, but also contribute significantly in increasing the carbon dioxide causing the effect of global warming. This project introduces an approach to discover sustainable and eco-friendly materials to be an alternative sound absorber by using kapok fiber as a natural material acoustic absorber Sound absorber samples from kapok fibers are fabricated and their acoustic properties are investigated through experiment. Good acoustic performance is found at 1.2 - 4.5 kHz with average absorption coefficient of 0.5.

1. INTRODUCTION

Noise is an environmental problem which greatly affects human health nowadays. Basically, the uses of sound absorber are necessary for the noise control for protect health and environmental quality. This study currently interest in developing sustainable absorbers made from natural material. In many architectural applications there is a need to absorb low-frequency noise, which is difficult to achieve by using porous sound-absorbing materials [1]. The utilization of synthetic materials act as acoustic absorbers is still connected in industry whereas these non-biodegradable causes contamination to nature. For instance, polyester fiber sound absorber demonstrates good quality of absorption property, while the chemically synthesized, it has the issue of high natural contamination and high cost [2]. Natural materials are characterized as materials from the natural world. Researchers have found that natural materials such as plant fibers, can be utilized to develop the sustainable sound absorbers [3] that help prevent noise pollution. Kapok fiber correlated to the seed hairs of the kapok tree (Ceiba pentandra) which is cellulosic fiber included its own characteristics consists of thin cell wall, large lumen, low density and hydrophobic-oleophilic properties which could adapt as absorbent material for sound and also including for oils, metal ions and dyes [4]. The aim of this project is construct the panel sound absorber and cylindrical shape casing using kapok fiber and being tested under reverberation chamber and impedance tube test respectively for investigate the acoustical performance of kapok fibers.

2. METHODOLOGY

2.1 Kapok fiber's testing sample preparation

The preparation of panel absorber (45cmx45cm) with 2cm thickness is shown in Figure 1. The preparation of 200g amount of kapok fiber needs to be loaded into the panel which will be tested in the reverberation chamber while Figure 2 shows that the cylindrical casing test sample that made by compressing certain amount of kapok fibers properly into the casing with the diameter of 3.3cm to be tested in impedance tube.

Figure 1 Example of panel frame of sound absorber (45cmx45cm) with 2cm thickness.

Figure 2 Example of cylindrical shape casing of 2cm thickness and 0.4g mass of kapok fiber.

2.2 Measurement of absorption coefficient

Experiment using reverberation room have been performed to determine the sound absorption coefficient by using ISO 354:2003 as reference. Sound produce from Audacity software through the speaker. Plus, the SLM device are used to obtain the data. The testing starts by placing the panel in the middle of reverberation room. The frequency range for this experiment is between 500 Hz to 5000Hz. The acoustical measurement system based on this experiment provided the result of the sound absorption coefficient at the one

and 1/3 octave frequency. The Figure 3 shows the diagram of reverberation chamber method setup.

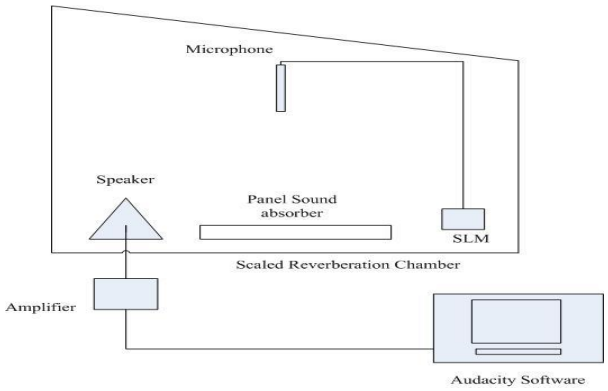

Figure 3 Diagram of reverberant method setup.

This impedance tube method by referring the EN ISO 10534-2 standard covers the use of an impedance tube, two microphone locations and a digital frequency analysis system. The loudspeaker feeds the white noise signal and test sample was placed at the removable cap. The utilization of RT Pro Photon analyzer which is to obtaining the data. Furthermore, the analysis of data which included the measurement of data are done by Matlab software. The frequency range for this experiment is between 500 Hz to 4.5 kHz. Figure 4 show the impedance tube method setup.

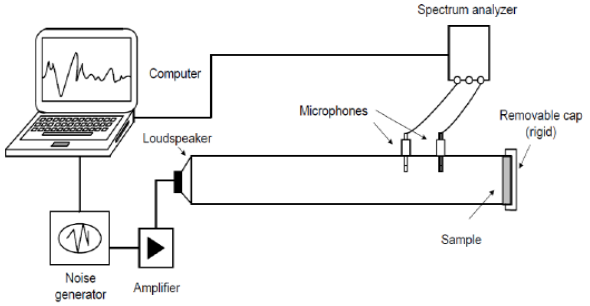

Figure 4 Measurement setup for the impedance tube.

3. RESULTS AND DISCUSSION

The Figure 5 shows the sound absorption coefficient of panel sound absorber for different speaker position testing which is speaker position 1 was placed against the panel meanwhile for speaker position 2 was placed directly to the panel. Both graph shows fluctuating trends which peak of sound absorption coefficient speaker 1 position is 0.5 at frequency range between 3000 and 3500 Hz. Meanwhile for speaker position 2 shows that the peak of sound absorption coefficient reaches 1.4 is twice which at frequency 1500 and 4000 Hz.

The figure 6 shows that the average absorption coefficient between speaker position 1 and speaker position 2. The graph shows fluctuating trends and reach peak of 1.6 at frequency 4000 Hz.

The figure 7 shows that the result of impedance tube test for cylindrical shape casing sample of 2cm thickness and 0.4 g mass of kapok fiber. The absorption coefficient is greater than 0.5 above 1000 Hz and approaches unity around 2000 and 2500 Hz.

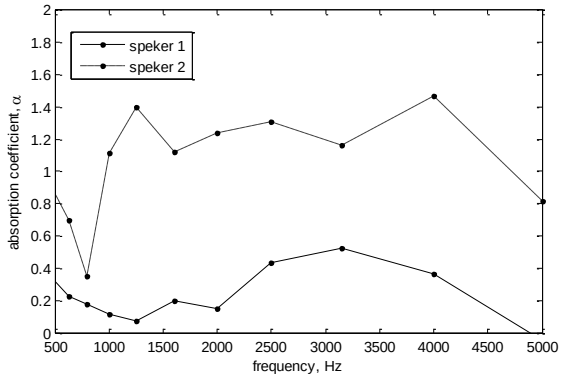

Figure 5 Absorption coefficient inside sealed chamber for speaker position 1 (-) and 2 (--).

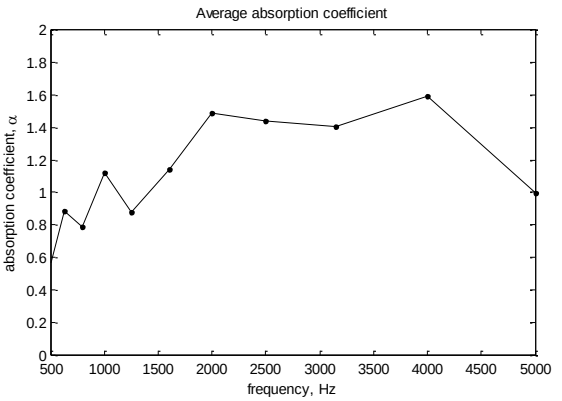

Figure 6 Average coefficient between speaker position 1 and 2 inside the sealed chamber.

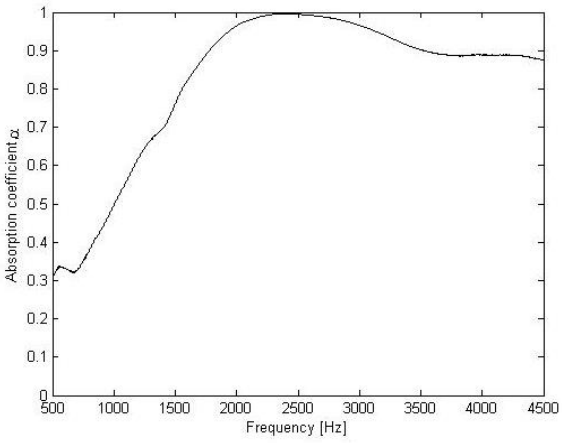

Figure 7 Impedance tube result for 2cm thickness and 0.4 g mass.

4. CONCLUSIONS

The acoustical properties of kapok fibers have been evaluated. The preliminary results show that the kapok fiber has good absorption coefficient.

ACKNOWLEDGEMENT

This research was supported by grant no. PRGS/1/2014/SS07/FKM/02/T0005.

REFERENCES

[1] J.P. Arenas and M.J. Crocker, "Recent trends in porous sound-absorbing materials," *Sound & Vibration*, vol. 44, no. 7, pp. 12-18, 2010.

[2] P. Limin, B. Song, J. Wang and D. Wang, "Mechanic and acoustic properties of the sound-absorbing material made from natural fiber and polyester," *Advances in Materials Science and Engineering*, vol. 2015, pp. 1-5, 2015.

[3] F. Asdrubali, "Survey on the acoustical properties of new sustainable materials for noise control," in *Proceedings of Euronoise*, 2006, pp. 1-10.

[4] Y. Zheng, J. Wang, Y. Zhu, A. Wang, "Research and application of kapok fiber as an absorbing material: A mini review," *Journal of Environmental Sciences*, vol. 27, pp. 21-32, 2015.

Improved fuzzy-PID controller in following complicated path for LEGO Mindstorms NXT

Nurul Nadirah Mohamad Khairi*, Sharifah Sakinah Syed Ahmad, Abdul Samad Shibghatullah

Faculty of Information Technology and Communication, Universiti Teknikal Malaysia Melaka, Hang Tuah Jaya, 76100 Durian Tunggal, Melaka, Malaysia

*Corresponding e-mail: nurulnadirahkhairi@gmail.com

Keywords: LEGO Mindstorms NXT; improved fuzzy-PID; complicated path

ABSTRACT – This research presents an application of improving fuzzy-PID controller method in controlling LEGO Mindstorms NXT while following the complicated path with more accurate and high velocity. LEGO Mindstorms NXT with single light sensor is used as a line follower robot to tracking the complicated black line drawn on the white surface.

1. INTRODUCTION

Line following is one of the most practical application as it sanctions the robot to moving from one point to another to perform tasks as previous study [1]. The situations become worst when robots need to follow the complicated and small thickness of line such as thin sharp curve line. The existing methods to control line following robot is still being issue on how to improve the performance of line follower robot. The traditional algorithm for line follower robot movement is, it will turn left when there is no line detected by the sensor and it will turn right when the line is detected by the sensor. This algorithm is very slow and not accurate, wasting valuable time and battery power. Line follower robot algorithm using conventional PID is much better than the earlier algorithm but the robot still will be unsteady about the line. Mas Pratama et al. [2] stated that the disadvantages of PID control system is, if given light sensor value are increasingly sensitive the response will overshoot and undershoot. However, if the light sensor value is made less sensitive to the response, there will be a recovery process which takes longer. So will cause the movement of robots are increasingly chaotic and unstable. On other hand, Hagras [3] found that to design a robust controller which can provide copacetic performance in the face of skeptical and imprecision, fuzzy logic controller is credited with being an adequate methodology.

As shown in Figure 1, the research step is commencing by elucidating the research question. The generic issues of the subject being studied are factors out and analysed. The alternative solution to the issues is list out and ordered based on their priority. The clarification of research question involved with theoretical study and exploratory study. There are two main components that involved during the research experimental as following

a) Complexity and thicknesses of line

There are two level of thicknesses in this research which the large and small thickness of pre-defined path. We add the zigzag line; sharp curve line and 'L' shape line to make the track is complicated to be followed by the LEGO Mindstorms NXT.

b) Improved fuzzy-PID controller

The performance of the improved controller method is formulated and modelling to evaluate the performance of the improved fuzzy-PID controller.

2. METHODOLOGY

2.1 Research framework

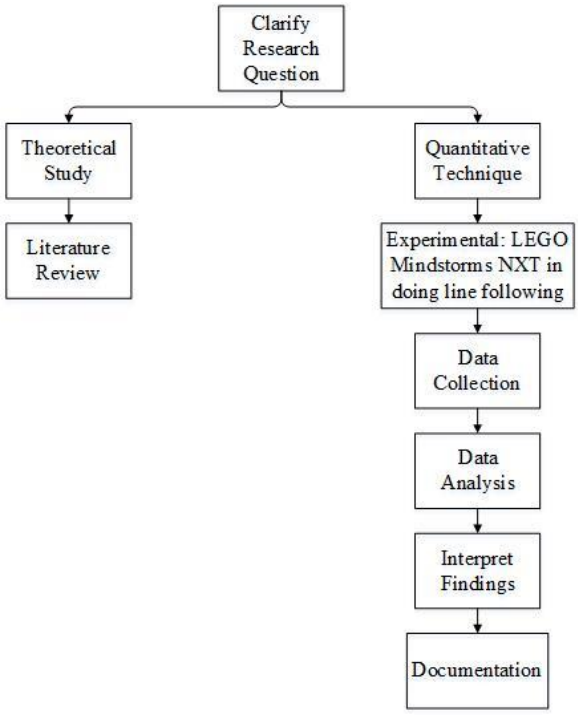

Figure 1 The process flow of the research.

3. RESULTS AND DISCUSSION

This section describes the analysis of the validation from the experiment. The analysis is divided into two part where the first part will discuss and analysed the findings when the LEGO Mindstorms NXT is following the large thickness of the pre-defined path using Boolean logic, PID controller, fuzzy logic controller, non-improved fuzzy-PID controller and improved fuzzy-PID controller. The second part will discuss and analysed the findings when the LEGO Mindstorms NXT is following the small

thickness of the pre-defined path using Boolean logic, PID controller, fuzzy logic controller, non-improved fuzzy-PID controller and improved fuzzy-PID controller. In this research, the different between non-improved fuzzy-PID controller and improved fuzzy-PID controller are non-improved fuzzy-PID controller is a normal fuzzy-PID controller method that has been used by the researcher while the improved fuzzy-PID controller is the proposed fuzzy-PID controller method that will improve the accuracy and velocity of the robot movement.

Table 1 Summarization of experimental result validation for large thickness of pre-defined path.

Method	Large Thickness (3.5 cm width of black tape)		
	Accuracy (%)	Time (s)	Velocity (cm/s)
Boolean Logic	20	60	15.24
PID Controller	47	59	15.50
Fuzzy Logic Controller	57	44	20.78
Non-Improved Fuzzy-PID Controller	70	37	24.71
Improved Fuzzy-PID Controller	77	33	27.70

Table 1 shows the summary of the evaluation and validation result from the experimental approach for the large thickness of pre-defined path. The column of accuracy and velocity validate the implementation of the improved fuzzy-PID controller is successful in which for all controller methods evaluated, improved fuzzy-PID controller method achieve the best result compared to other methods. The result validates that velocity of the LEGO Mindstorm NXT robot is high when follow the big thickness of pre-defined path.

Table 2 Summarization of experimental result validation for small thickness of pre-defined path.

Method	Small Thickness (1.75 cm width of black tape)		
	Accuracy (%)	Time (s)	Velocity (cm/s)
Boolean Logic	13	0	0
PID Controller	23	0	0
Fuzzy Logic Controller	30	0	0
Non-Improved Fuzzy-PID Controller	80	35	26.13
Improved Fuzzy-PID Controller	93	25	36.58

Table 2 shows the summary of the evaluation and validation result from the experimental approach for small thickness of pre-defined path. The column of accuracy and velocity validate the implementation of the improved Fuzzy-PID controller is successful in which for all controller methods evaluated, improved fuzzy-PID controller method achieve the best result of velocity. As shown in Table 2, only non-improved fuzzy-PID controller and improved fuzzy-PID controller method successful finish follow the pre-defined path where the time taken to finish tracking the small thickness of pre-defined path for each method is 35 second and 25 second. Although non-improved fuzzy-PID controller successful finish tracking the small thickness of pre-defined path, however, improved fuzzy-PID controller method achieve the best result compared to other methods. The result also validates that velocity of the LEGO Mindstorm NXT robot is faster when following the small thickness of pre-defined path compared the large thickness of pre-defined path.

4. CONCLUSIONS

Usually, line follower robot might be able to follow the narrow and simple curve line, but with sharp curve line and zigzag line, the pattern of LEGO Mindstorms NXT robot movement will be not accurate and slow. The high complexity of line that is sharp curve line and zigzag line indeed give influence in robot movement. Only fuzzy-PID controller method can tracking all type of the line whether in large or small thicknesses of the line. At the end of the experiment, zigzag line and sharp curve line is identify as the type of line that will make robot movement is not accurate, chaotic and slow. Although the only single light sensor is installed in LEGO Mindstorms NXT, however, when the robot is controlled by the improved fuzzy-PID controller method, the robot can follow the path more accurate and faster.

The methods that have been used to make a comparison with the improved fuzzy-PID controller are Boolean logic, PID controller, fuzzy logic controller, and non-improved fuzzy-PID controller. By using Boolean logic, the robot movement is very inaccurate and slow. It is a very traditional method for line follower robot and suitable for beginner to learn about line follower robot. PID controller and fuzzy logic method make the robot movement also inaccurate but better than Boolean logic method. As a mention earlier, although a non-improved fuzzy-PID controller successful finish tracking the small thickness of pre-defined path, however, improved fuzzy-PID controller method achieve the best result which is the robot can follow all complicated path with high accuracy and velocity.

REFERENCES

[1] M. Pakdaman and M.M. Sanaatiyan, “Design and implementation of line follower robot,” in *Second International Conference on Computer and Electrical Engineering TCCEE*, 2009, pp.585-590.

[2] I.P.A. Mas Pratama, I.N. Suweden and I.B. Alit Swamardika, “Sistem kontrol pergerakan pada robot line follower berbasis hybrid PID-fuzzy logic,” in *Proceeding Conference on Smart-Green Technology in Electrical and Information Systems,* 2013, pp. 159-164.

[3] H. Hagras, “Type-2 FLCs: A new generation of fuzzy controllers,” *IEEE Computational Intelligence Magazine*, vol. 2, no. 1, pp. 30–43, 2007.

Numerical studies on vibration characteristics on ball bearing operated under hexagonal boron nitride (hBN) nanoparticles

N.S.R. Apandi[1], R. Ismail[1,2,*], M.F.B. Abdollah[1,2]

[1)] Faculty of Mechanical Engineering, Universiti Teknikal Malaysia Melaka,
Hang Tuah Jaya, 76100 Durian Tunggal, Melaka, Malaysia
[2)] Centre for Advanced Research on Energy, Universiti Teknikal Malaysia Melaka,
Hang Tuah Jaya, 76100 Durian Tunggal, Melaka, Malaysia

[*]Corresponding e-mail: rainah@utem.edu.my

Keywords: Finite element analysis, vibration characteristic, ball bearings, hexagonal boron nitride

ABSTRACT – This paper presents a simulation approach on the vibration responses of a bearing system with different volume of concentration of hexagonal boron nitride (hBN) nanoparticles mixed with diesel engine oil. A 3D finite element model of bearing system is numerically solved within ANSYS WORKBENCH 16.0 solver. The characteristic frequency is distinguished between new bearing, 0.5 mm outer defected bearing and 0.5 mm inner defected bearing. The simulation results show that the hBN nanoparticles function as an additive gives lowest value of vibration amplitudes to the bearing system.

1. INTRODUCTION

Ball bearing can play an important role in addressing the issue of noise and vibration generators due to the imperfection of geometrical bearing components, rotation of the lubricated contacts, stiffness in the bearings and parametric excitations. The performance of machine is also limited by the frequency of bearing failure compared to the other components [1]. Therefore, new additives in the lubricants has become one of the important research because the additives presence in the lubricants can helps to reduce wear and friction between the contacting surfaces. In previous study, it was found that hBN nanoparticles can act as promising additives in reducing the wear and friction [2]. However, there is no significant research done on the performance of hBN nanoparticles in reducing the vibration amplitude. Thus, in this paper the vibration amplitude is studied through the simulation approach by using ANSYS WORKBENCH 16.0.

2. METHODOLOGY

The hexagonal boron nitride (hBN) nanoparticles is in the form of white powder and dispersed in conventional diesel engine oil (SAE 15W40). Further discussion about the sample preparation can be referred in the previous paper published by Apandi et al. [3]. In this analysis friction force, F_f is used to represent the friction that happens between the nanoparticles and contact surface of the bearing element. The F_f can be obtained by conducting the tribological testing to determine the coefficient of friction (COF) using a four-ball tester. The procedure is followed the standard test which is ASTM D4172. The COF value is acquired for hBN mixed lubricant with 0.0 vol% and 0.2 vol% of concentration of hBN. In order to simplify the modelling and analysis, the bearing and shaft are the only part to be analyzed. All components (outer ring, inner ring, balls and cage) of the bearings system are modelled as rigid body. The bearing model is subjected to rotational speed and friction force at the reference point of outer ring.

2.1 Finite element method (FEM)

FEM has been carried out by using ANSYS WORKBENCH 16.0 package. 6206 deep groove ball bearing and a shaft are drawn in CATIA software and the complete model is imported to the ANSYS software. The structural steel bearing system is modelled as deformable body by using the material properties which are density, ρ = 7800 kg/m^3, the modulus elasticity, E = 206 GPa and Poisson's ratio, υ = 0.33. The artificial defect on inner and outer element are also created in the CATIA software. Overall, there are three bearing conditions are taken into consideration for the analysis which are new bearing, outer defected bearing (1x0.5) mm and inner defected bearing (1x0.5) mm as shown in Figure 1 and Figure 2.

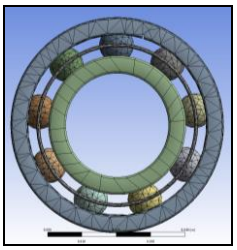

Figure 1 Meshed model of 0.5 mm outer race defect.

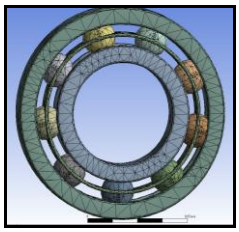

Figure 2 Meshed model of 0.5 mm inner race defect.

There are two types of analysis are done in this

project which are Modal analysis and Harmonic Response analysis. The results are obtained in frequency domain response. In meshing part, outer and balls element are using Tetrahedron (Solid 168) free meshing and the rest are using free mapped meshing Hexahedron (Solid 164). Each bearing element, edge sizing with number of division of 100 and bias factor of 5 is applied on the model. The behavior of meshing is hard type and the total number of nodes is 126378 with number of elements is 56947. The frequency response is captured at the point on top of the defected area of inner and outer element.

3. RESULTS AND DISCUSSION

The analysis is done with the constant value of moment applied 5 Nm which is represent the input torque from the motor. The frictional force calculated is equal to 1.8 N and 2.0 N for the conventional diesel engine oil and 0.2 vol% of concentration mixed with diesel engine oil, respectively. Following are the frequency domain graphs from the ANSYS WORKBENCH 16.0 for all bearing conditions.

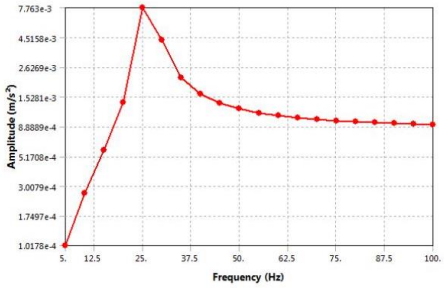

Figure 3 Vibration amplitude of the new bearing.

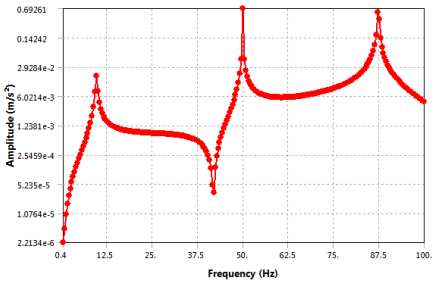

Figure 4 Vibration amplitude of outer defected bearing.

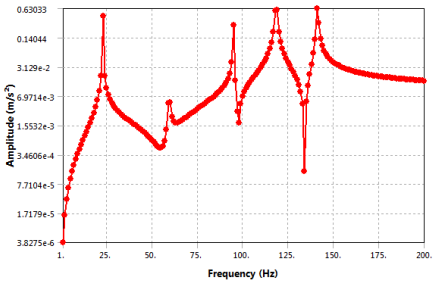

Figure 5 Vibration amplitude of inner defected bearing.

Figure 3, 4 and 5 indicate the vibration response for new bearing, outer defected bearing and inner defected bearing, respectively. From Figure 3, it is clearly shown that the significant peaks of fundamental frequency of the bearing system. Meanwhile, for the outer and inner defected bearing the results shown that the stronger impact wave with the more non-synchronous peak compared to the new bearing as shown in Figures 4 and 5. The data from the simulation is tabulated in Table 1. Table 1 also shows the percentage of reduction of amplitude of concentration in every condition of bearing. It is proven that 0.2 vol% of hBN gives the lowest vibration amplitude compared to the 0.0 vol% of hBN.

Table 1 Amplitude of bearing characteristic frequency.

Types of bearing	Amplitude (ms^{-2})		Amplitude reduction (%)
	0.0 vol% of hBN	0.2 vol% of hBN	
New bearing	0.0097	0.0078	19%
Outer defected bearing	0.4191	0.3878	7%
Inner defected bearing	0.0145	0.0124	14%

4. CONCLUSION

This paper proposes a finite element approach accordingly to determine the performance of hBN nanoparticles in reducing the vibration amplitudes of new and defected bearings. It can be concluded that the hBN with 0.2 vol% of concentration gives lower value of vibration amplitude compared to the conventional diesel engine oil for all types of bearing condition. This is because the manometer size of nanoparticles makes it easily to enter the surface of defected area. It also found that the vibration amplitude for outer defected bearing is higher than the inner defected bearing. This is because the outer race defect is remained at the load zone at the maximum position meanwhile inner race defect moves in and out of the load zone. The strong vibration amplitude occurs in the load zone while the weaker vibration amplitude is produce as the defect is outside the load zone.

ACKNOWLEDGEMENT

This research was supported by grant no. RAGS/1/2014/TK01/FKM/B00066.

REFERENCES

[1] N. Dhanush, G. Dinesh, V. Perumal, S.R. Mohammed and A.L. Nafez, “Analysis of deep groove ball bearing using vibrational parameters,” *International Journal of Engineering and Technology*, vol. 4, no. 3, pp. 98-109, 2015.

[2] M.I.H.C. Abdullah, M.F.B. Abdollah, H. Amiruddin, N. Tamaldin and N.R. Mat Nuri, “Effect of hBN/Al_2O_3 nanoparticle additive on the tribological performance of engine oil,” *Jurnal Teknologi (Sciences and Engineering)*, vol. 66, no. 3, pp. 1-6, 2014.

[3] N.S.R. Apandi, R. Ismail and M.F.B. Abdollah, “Vibration characteristic on ball bearing operated with hexagonal boron nitride (hbn) nanoparticle mixed with diesel engine oil,” in *Proceedings of 4th Malaysia-Japan Tribology Symposium*, 2016.

Vibration analysis of centrifugal pump caused by impeller erosion

R.M. Dan[1,2,*], A.H.A. Hamid[1,2], M.A. Seron[1], A. Putra[1,2], R.K. Mazlan[1,2]

[1)] Faculty of Mechanical Engineering, Universiti Teknikal Malaysia Melaka,
Hang Tuah Jaya, 76100 Durian Tunggal, Melaka, Malaysia
[2)] Centre for Advanced Research on Energy, Universiti Teknikal Malaysia Melaka,
Hang Tuah Jaya, 76100 Durian Tunggal, Melaka, Malaysia

[*]Corresponding e-mail: reduan.dan@utem.edu.my

Keywords: Vibration analysis; impeller erosion; contamination

ABSTRACT – The focus of this research is to investigate the erosion of impeller through vibration analysis. Solid contaminants were introduced in the pump system to accelerate the wear rate of the impeller. In this study, accelerometer is used to measure the vibration of the pump per time. Mass removal of the impeller is measured to correlate with the vibration signal of the impeller during operation. It is discovered that the wear of the impeller through observation of mass removal correlates with the vibration signal of the impeller during operation.

1. INTRODUCTION

Erosion of the impeller is a common problem that occurs when the pump medium contains suspended particles due to dissolved contaminants. Prevention is a given in order for a longer operation time for the centrifugal pump. Vibration analysis is extensively used as a tool for condition base monitoring of machine. Several studies have focused on the vibration analysis of centrifugal pump [1-4].

Every contacting surfaces that involves mechanical actions experiences wear due to gradual removal of particles of the contacting surfaces' material which obviously applies to gearing systems. It is generally accepted that wear can be subcategorised into the adhesive wear, abrasive wear, corrosive wear, surface fatigue wear and deformation wear [5-7]. The wear that pump impeller experiences is due to contacting surface of the impeller and the fluid that passes through causing cavity and erosion. Vibration analysis is extensively researched on other literatures however, correlation with the wear of the wear of the impeller is not research intensively due to vibration analysis being accurate for determination of the wear mode.

Thus, the objective of this study is to investigate the erosion of the impeller through the correlation of the vibration analysis and the wear of the pump.

2. METHODOLOGY

2.1 Pump system

The pump system consists of a centrifugal pump with specifications shown in Table 1. A flow system configuration is constructed with the centrifugal pump connected to the water sump using piping as seen in Figure 1. Accelerometer sensor is connected to the pump casing to measure the displacement signal per time. The signal is then analysed through VibraQuest Pro.

Table 1 Centrifugal pump specification.

Specification	Value
Power (HP)	0.5
Q. max (L/min)	35
H. max (m)	35
Suction max (m)	9
Speed (rpm)	2850

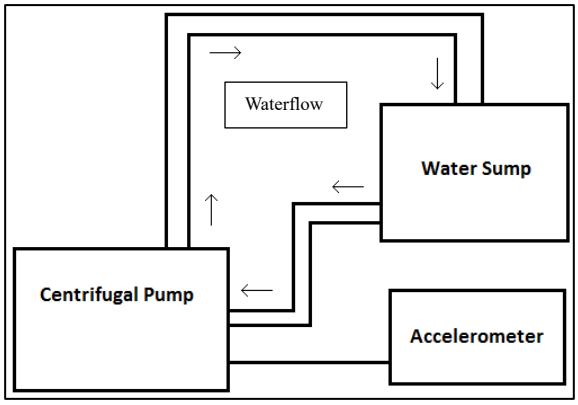

Figure 1 Pump system schematic diagram.

2.2 Impeller frequency

The measured signal is in a time waveform which does not specify the exact vibration signal of the impeller. Thus, the time waveform needs to be converted into spectrum signal using Fast Fourier Transform (FFT) and the impeller frequency is calculated using Equation (1):

$$Impeller\ Frequency = \frac{Number\ of\ impeller\ blades \times RPM}{60} \quad (1)$$

where the calculated impeller frequency obtained is at 1710 Hz.

2.3 Impeller wear

The impeller is weighed per time to obtained the wear per time. This is done to make a comparison with the vibration measurement and the wear of the impeller. Wear is generally known as the process of gradual particle removal or displacement through the contacting surfaces' material. These gradual removals of particle

can be associated to the reduced mass of the specimen as the displaced particles are removed from its interaction with operating fluid of the pump.

3. RESULTS AND DISCUSSION

The impeller mass and vibration is measured for 1-hour interval until the 5th hour of pump operation. The result obtained for the impeller mass and vibration is plotted as seen in Figure 2 and Figure 3 respectively.

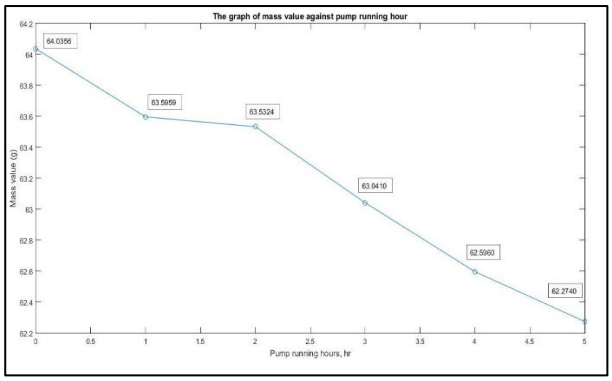

Figure 2 Graph of impeller mass against time.

Figure 2 shows that the mass of the impeller gradually decrease over the time. It shows that the fine sand has eroded the impeller of the pump due to the friction force between the sand and the surface of the impeller and it makes the pump impeller have some scratches and some of the impeller vane has fractured. It can be said that; the deterioration of the pump impeller can increase the level of the pump vibration due to the unbalance of the pump impeller. The high level of pump vibration will affect the efficiency and performances of the pump besides it can danger to the public if maintenance is not carried out.

For the first, 2nd and 3rd hour of pump operation, the vibration signal begins to increase albeit insignificantly towards the wear rate of the impeller. The trend has dramatically increased from impeller defect of 3 hours running to 5 hours running and it shows that the vibration has given more impact on the pump which can harm to the pump itself. It is due to the friction between the sand and pumps impeller that caused the material of the impeller to be worse. By keeping the worse condition of the impeller, the high probability of unbalance of the pump impeller can be happened. When this phenomenon continues, it can be severe damage especially on the pump cover, pump bearing and pump seal that cause the leaking of the pump. Hence, it will shorten the life of the pump itself.

The vibration severity as per ISO 10816 states that for small machine that the magnitude of the vibration of 0.0089 which is in the range of <0.01 pk (in/s) is still in a good condition.

4. CONCLUSION

The investigative study leads to various results where it is found that the vibration analysis correlates with the wear of the impeller through mass removal. This suggested that the vibration analysis is a reliable tool for determining the characteristic of the wear. Although the experiment has not reach a significant wear of the impeller, it is concluded that the impeller has reached an exponential wear.

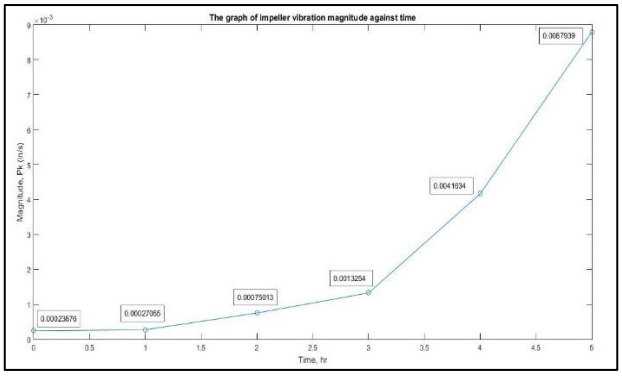

Figure 3 Graph of vibration magnitude against time.

REFERENCES

[1] R. Podugu, J.S. Kumar and N.S Kumar, "A modal approach for vibration analysis and condition monitoring of a centrifugal pump," *International Journal of Engineering Science and Technology*, vol. 1, no. 3, pp. 6335-6344, 2011.

[2] A.R. Mohanty, P.K. Pradhan, N.P. Mahalik and S.G. Drastier, "Fault detection in a centrifugal pump using vibration and motor current signature analysis," *International Journal of Automation and Control,* vol. 6, no. 3-4, pp. 261-276, 2012.

[3] A. Suhane, "Experimental study on centrifugal pump to determine the effect of radial clearance on pressure pulsations, vibrations and noise", *Int. J. Eng. Res. Appl*, vol. *2*, no.4, 1823-1829, 2012.

[4] S. Farokhzad, N. Bakhtyari and H. Ahmadi, "Vibration signals analysis and condition monitoring of centrifugal pump", *Technical Journal of Engineering and Applied Sciences*, pp. 1081, 2013.

[5] J.T Burwell Jr., "Survey of possible wear mechanisms", *Wear*, Vol. 1, pp. 119-141, 1957.

[6] J.A Collins, "Mechanical design of machine elements and machines: A failure prevention perspective", Hoboken, NJ: Wiley, 2010.

[7] M.B. Peterson, M.K. Gabel and M.J. Derine, "Understanding wear", *ASME Standardization News*, vol. 2, no. 9, pp. 5-32, 1974.

Vibration analysis of ball bearing using Finite Element Analysis

N.S.R. Apandi[1], R. Ismail[1,2,*], M.F.B.Abdollah[1,2]

[1)] Faculty of Mechanical Engineering, Universiti Teknikal Malaysia Melaka,
Hang Tuah Jaya, 76100 Durian Tunggal, Melaka, Malaysia
[2)] Centre for Advanced Research on Energy, Universiti Teknikal Malaysia Melaka,
Hang Tuah Jaya, 76100 Durian Tunggal, Melaka, Malaysia

[*]Corresponding e-mail: rainah@utem.edu.my

Keywords: Bearing vibration analysis; Finite Element Method; ball bearing

ABSTRACT – This paper presents a numerical approach on the frequency characteristics of a new and defected bearings. A 3D model of bearing system with 0.5 mm artificially defects including outer and inner race was modelled by using CATIA software. The numerical simulation was completed by employing ANSYS WORKBENCH 16.0. The simulation result shows the existence of significant and non-synchronous peaks which represent the new and defected bearing defaults with the frequency characteristics of the system.

1. INTRODUCTION

Ball bearing provides a rotational freedom and relative positioning while transmitting a load between two contact surfaces with a minimum friction [1]. Over the time, bearing failure will lead to mechanical system breakdown because of the misalignment, defect on bearing elements, unsuitable lubricants, and unbalanced force. Eventually, these problems will become a reason for undesirable vibration. This phenomenon can be examined from the early stages of bearing defects. The defects that occur on bearing element such as inner race, outer race and ball spin can be detected by their own vibration frequency characteristic. Monitoring and analysing the vibration signal of the bearing defects give researchers the fastest way to distinguish the existence of faults and the worseness of the system condition. As stated in paper published by Liu et al. [2] the localized defects can propagate the effects on the speed, radial load, and defect shape in pulse waveform characteristic. The other studies were also conducted by Li et al. [3] and Singh et al [4] which using explicit dynamic finite element analysis to study the vibration characteristic of rolling bearing. However, there is no significant studies which using the Modal and Harmonic Response analysis to analyse the vibration characteristic of rolling bearing. Thus, in this study the vibration characteristics of a bearing defect is obtained when bearing system is operated under hBN nanoparticles mixed with diesel engine oil lubricant through ANSYS WORKBENCH 16.0.

2. METHODOLOGY

Bearing system consists of a single deep groove ball bearing 6206 and the shaft with a length of 500 mm are modelled in CATIA software. The artificial defect of 0.5 mm hole is also created on the inner and outer race of bearing element. The focus of this paper was to determine the vibration characteristic on the new and defected bearings. Hence, a structural steel bearing system is modelled as deformable body by inserting the material properties density, ρ = 7800 kg/m^3, the modulus elasticity, E = 206 GPa and Poisson's ratio, υ = 0.33. For simulation purpose, three conditions are taken into consideration which are new bearing, 0.5 mm outer defected bearing and 0.5 mm inner defected bearing as shown in Figure 1. The detailed dimension of the bearing model was also shown in Table 1.

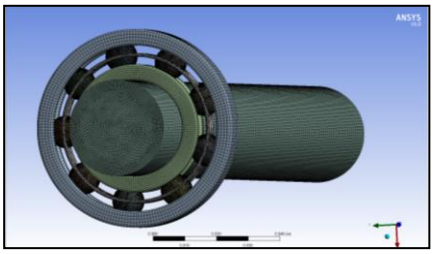

(a)

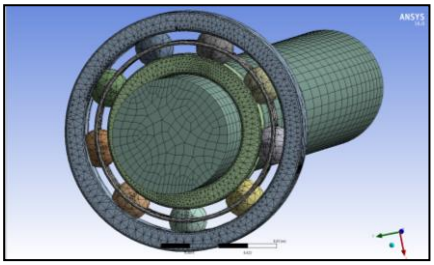

(b)

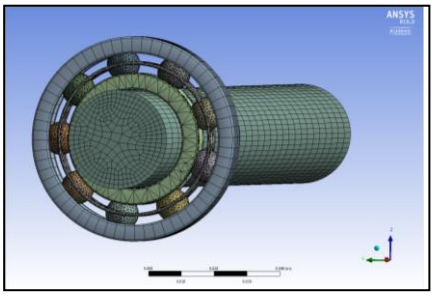

(c)

Figure 1 The meshed model for bearing system. (a) Meshed model of new bearing, (b) meshed model of 0.5mm outer defected bearing and (c) meshed model of 0.5 mm inner defected bearing.

Table 1 Dimensions of bearing system model.

Feature name	Dimension (mm)
Outer diameter, OD	62.0
Inner diameter, ID	30.0
Ball diameter, D	8.0
Pitch diameter, PD	35.6
Breadth, B	16.0
Ball number, N	9
Length of defect, Ld	0.50
Depth of defect, Dd	0.25
Shaft diameter, Os	30.0
Length shaft,Ls	500

In this analysis, the friction force, F_f which indicate the lubricant, is applied with the value of 2.0 N and 5 Nm of torque produced by DC motor.

2.1 Bearing frequencies

The physical defects can occur on bearing elements such as inner race, outer race, ball and cage. The defects will cause a high amplitude of vibration. Each element has variant characteristic frequencies such as fundamental frequency, ball spin outer frequency, (BPOF) and ball spin inner frequency, (BPFI) can be calculated by using the formula below:

$$BPFO = \frac{N_b}{2} f_s \left(1 - \frac{B_d}{P_d} \cos\phi\right) \quad (1)$$

$$BPFI = \frac{N_b}{2} f_s \left(1 + \frac{B_d}{P_d} \cos\phi\right) \quad (2)$$

where N_b is the number of balls, f_s is shaft speed in rpm, P_d is the pitch diameter in mm, B_d is ball diameter in mm and contact angle, ϕ. For the bearing model in this paper, the theoretical value for new bearing is 25 Hz, f_{BPFO} is 87 Hz and for the f_{BPFI} is 130 Hz.

3. RESULTS AND DISCUSSION

The frequency response graph for the new and defected bearings are shown in Figure 2.

From the theoretical formula, the defect frequencies can be detected by the significant peaks that appeared on the frequency graph. Particularly for BPOF, the non-synchronous peak is detected at 3X and BPFI is appeared at 5X non-synchronous peak. Meanwhile, the new bearing is observed at 1X significant peak which is equivalent to the fundamental frequency. From the simulation findings, it is found that the non-synchronous peaks which are 3X and 5X for both inner and outer defected bearings are noticed as theoretical value.

From Table 2, it is found that the frequencies from the simulations are similar with the theoretical values. It can be seen that significant peak on new bearing and non-synchronous peaks appeared on the inner and outer defected bearings shows good predictive agreement with the experimental results published by Apandi [5].

4. CONCLUSION

It is found that the proposed numerical approach is applicable to determine the early deterioration of the bearing system that occur in outer and inner race of bearing element.

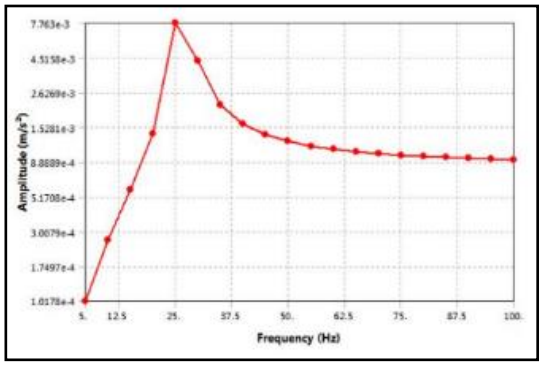

(a)

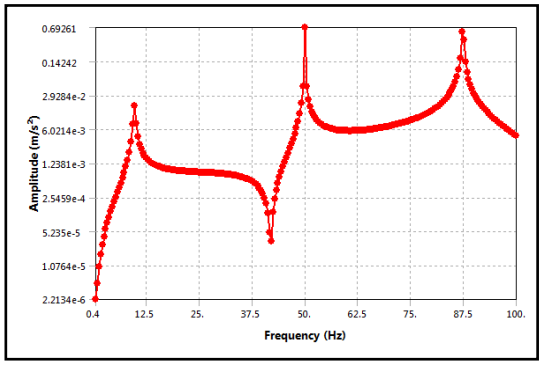

(b)

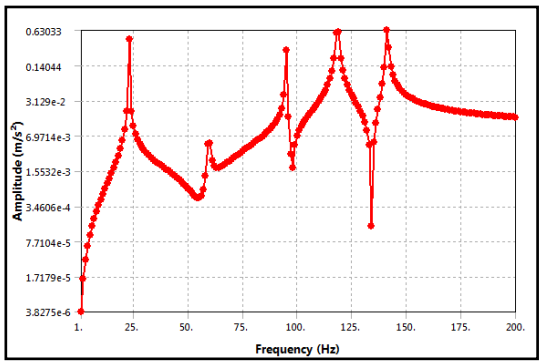

(c)

Figure 2 Frequency response graph of (a) new bearing, (b) outer defected bearing and (c) inner defected bearing.

Table 2 Bearing frequencies

Types of bearing	Peaks	Frequency (Hz)
New bearing	1X	25.0
Outer defected bearing	3X	89.7
Inner defected bearing	5X	130.5

ACKNOWLEDGEMENT

This research was supported by grant no. RAGS/1/2014/TK01/FKM/B00066.

REFERENCES

[1] N. Dhanush, G. Dinesh, V. Peruma, S.R. Mohammed and A.L. Nafez, "Analysis of deep groove ball bearing using vibrational parameters," *International Journal of Engineering and Technology*, vol. 4, no. 3, pp. 98-109, 2015.

[2] J. Liu, Y.M. Shao and M.J. Zuo, "The effects of the shape of localized defects in ball bearings on the vibration waveform," *Proceedings of the Institution of Mechanical Engineerings, Part K: Journal of Multi-body Dynamics*, vol. 227, no. 3, pp. 261-274, 2013.

[3] G.C. Li, W. Peng, Y.C. Li, L.X. Gao and J. Zhang, "Simulation and dynamic analysis of outer ring fault on rolling bearings using explicit finite element method," *China Mechanical Engineering,* vol. 23, no. 23, pp. 2825-2829, 2012.

[4] S. Singh, U.G. Kopke, C.Q. Howard and D. Peterson, "Analyse of contact forces and vibration response for a defective rolling element bearing using and explicit dynamics finite element model," *Journal of Sound and Vibration*, vol. 333, pp. 5356-5377, 2014.

[5] N.S.R. Apandi, R. Ismail and M.F.B. Abdollah, "Vibration characteristic on ball bearing operated with hexagonal boron nitride (hbn) nanoparticle mixed with diesel engine oil," in *Proceedings of 4th Malaysia-Japan Tribology Symposium*, 2016.

The identification and control of an upper extremity exoskeleton for motor recovery

Z. Taha, A.P.P.A. Majeed*, M.A. Abdullah, I.M. Khairuddin, M.A. Zakaria, M.H.A. Hassan

Innovative Manufacturing, Mechatronics and Sports Laboratory, Universiti Malaysia Pahang, 26600 Pekan, Pahang, Malaysia

*Corresponding e-mail: anwarmajeed@imamslab.com

Keywords: Rehabilitation; system identification; control

ABSTRACT – This paper presents the model identification and control of an upper-limb exoskeleton system. The exoskeleton is intended for the rehabilitation of the elbow joint. The input-output measurement i.e. current and angular displacement of the actuator is used to identify the model via MATLAB System Identification Toolbox. The identified plant is then used to perform the Hardware in the Loop (HIL) simulation to identify appropriate Proportional-Derivative (PD) control gains prior to its employment of the actual exoskeleton system. It was established that the exoskeleton is able to track the joint trajectory prescribed with an acceptable error bounded between+/-2°.

1. INTRODUCTION

Approximately 21,000 stroke cases are reported each year in Malaysia, causing 2,000 deaths and 19,000 significant disabilities [1]. More often than not, patients who survived this acute event are left with a considerable residual disability. They, in turn, would essentially require assistance with activities of daily living (ADL). Studies have shown that continuous rehabilitation may significantly increase one's mobility and this could be achieved through the use of robotics [2].

The present study aims at identifying an appropriate model for the control of an upper-limb exoskeleton system. The exoskeleton is designed to rehabilitate the flexion and extension of the elbow joint. A HIL simulation is performed prior to assessing suitable control gains, specifically the PD gains prior to its implementation on the hardware. The performance of the system is also assessed.

2. METHODOLOGY

The exoskeleton system is shown in Figure 1(a). In this study, a sinusoidal signal with an amplitude of 90° and a frequency of 0.5 rad/s for a period of 30 seconds is supplied to the system. The angular displacement of the 12V DC motor (rated current of 15A) (Cytron) attached at the exoskeleton elbow joint is measured by means of a potentiometer (Honeywell 53C3 20k). MD 30C 30A (Cytron) motor driver is used to regulate the motion of the DC motor. The input measurement, i.e. current value is measured via a current sensor (BB-ACS756). Arduino Mega 2560 is used as the data acquisition (DAQ) device. The controller unit is shown in Figure 1(b). MATLAB Simulink Arduino Support Package was used to calibrate the sensors as well as recording the data.

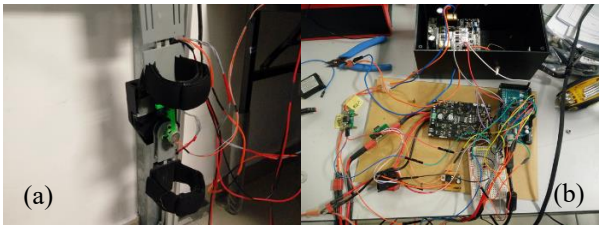

Figure 1 (a) Exoskeleton unit and (b) controller unit.

MATLAB System Identification Toolbox is used to ascertain the model of the system based on the recorded input-output measurements [3]. Figure 2 depicts the measurement data. Approximately 70% of the data is used for the estimation process, whilst the remaining 30 % of the data is utilised for the validation process. A number of continuous transfer function (ctf) were estimated by varying the number of zeros and poles of the system. AzBp, where A corresponds to the number of zeros whilst B the number of poles. Furthermore, a second order state-space model was also estimated. All the estimation and validation fit of the estimated models are evaluated.

Once the appropriate model is acquired, the identified model is used to perform the HIL simulation via MATLAB Simulink, in which in this study, the appropriate PD-controller gains are heuristically tuned to provide satisfactory joint trajectory tracking. The tuned PD gains are then used on the hardware, and the performance of the system is evaluated.

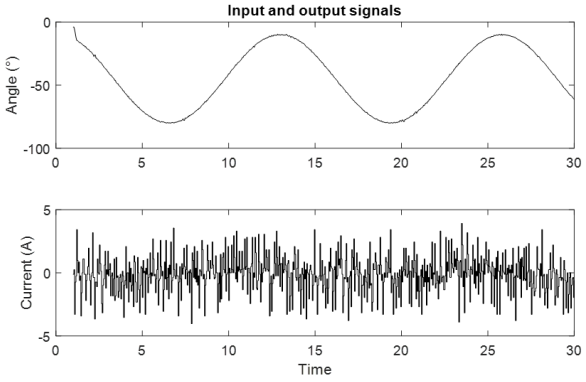

Figure 2 Measured input-output data.

3. RESULTS AND DISCUSSION

It could be observed from Figure 3 (estimation) and Figure 4 (validation), that the ctf(0z2p) model fits well in both the estimation (97.7%) and validation (97.66%) stage. The ctf(0z2p) equation as follows:

$$G(s) = \frac{477.3}{s^2 + 0.08299\,s + 367.4} \quad (1)$$

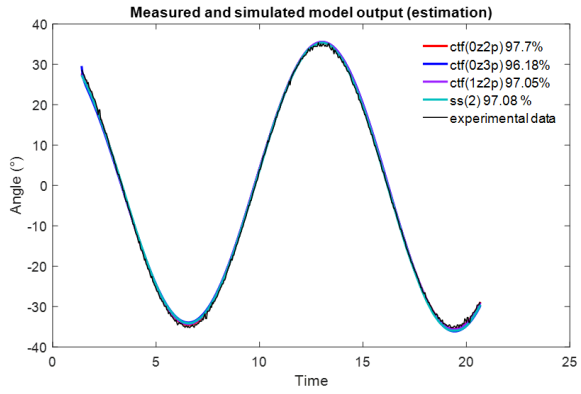

Figure 3 Model estimation.

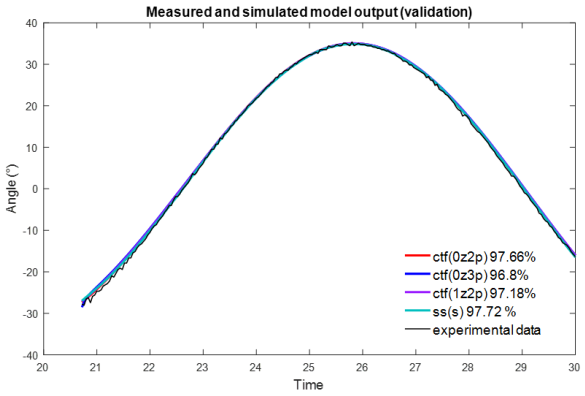

Figure 4 Model validation.

The PD gains heuristically tuned from the identified model are 50.9921 and 0.7242 for K_p and K_d, respectively. The response of the HIL simulated system is depicted in Figure 5, whilst the experimental run of the tuned parameters on the hardware is shown in Figure 6. The error between the reference signal and the experimental response is illustrated in Figure 7. It is evident that the controller works arguably well as the error is bounded between +/- 2°.

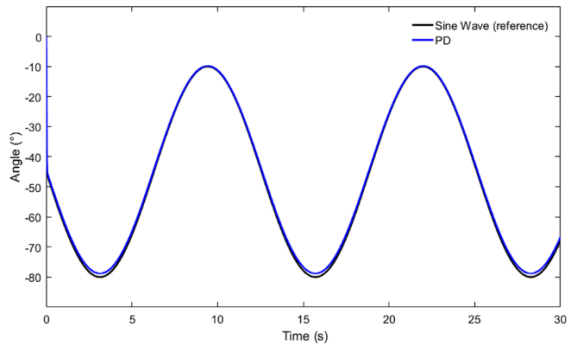

Figure 5 HIL simulation results.

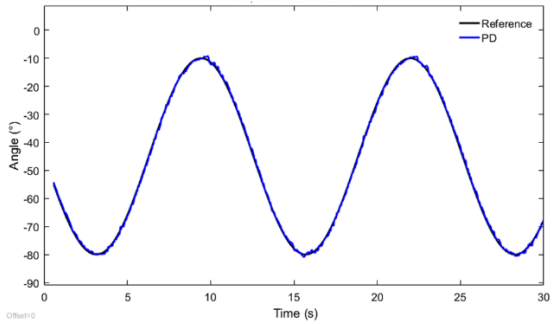

Figure 6 Experimental results.

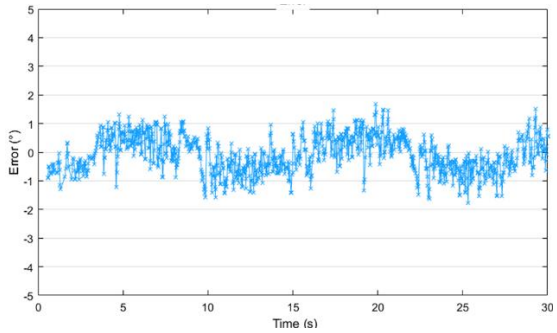

Figure 7 Response error.

4. CONCLUSION

The study examines the identification and control of an upper extremity exoskeleton that performs the flexion and extension of the elbow joint. The transfer function of the system was successfully identified. A HIL simulation was carried out to obtain suitable controller gains, and the gains were implemented in the actual hardware. It was found that the simulation and experimental results were in good agreement. Future works will include the incorporation of Active Force Control (AFC) to the existing controller to investigate its effectiveness in attenuating disturbances.

ACKNOWLEDGEMENT

The authors would like to thank Universiti Malaysia Pahang for providing the grant (RDU160375) in supporting this research.

REFERENCES

[1] S.N. Nazifah, I.K. Azmi, B.B. Hamidon, I. Looi, A.A. Zariah and M.R. Hanip, "National stroke registry (NSR): Terengganu and Seberang Jaya experience," *Med. J. Malaysia*, vol. 67, no. 3, pp. 302–304, 2012.

[2] Z. Taha, A.P.P.A. Majeed, M. Yashim and W. Paul, "Modelling and control of an upper extremity exoskeleton for rehabilitation," *IOP Conf. Ser. Mater. Sci. Eng.*, vol. 114, no. 1, pp. 12134, 2016.

[3] L. Ljung and R. Singh, "Version 8 of the MATLAB system identification toolbox," *IFAC Proc. Vol.*, vol. 45, no. 16, pp. 1826–1831, 2012.